JOURNAL OF MATERIALS SCIENCE **38** (2003) 4677–4695

Ceramic membranes: Morphology and transport

H. VERWEIJ
Department of Materials Science & Engineering, Ohio State University, 2041 College Road, Columbus, OH 43210-1178, USA
Internet: www.mse.eng.ohio-state.edu/fac_staff/faculty/verweij/
E-mail: verweij@mse.eng.ohio-state.edu

Ceramic membranes generally consist of permselective material as standalone disks or tubes or as thin films on porous supports. Applications are often energy/environment-related in H_2, CO_2 and O_2 separation, H_2O pervaporation, hydrocarbon separation/partial oxidation and liquid treatment such as water purification. Thin membrane films can be applied on porous supports by particulate, wet-chemical or vapor phase deposition techniques. Examples of permselective inorganic membrane compositions are *dense* Pd alloys and various perovskites, *micro-porous* ($Ø < 2$ nm) amorphous silica and zeolites and *meso-porous* ($2 < Ø < 50$ nm) alumina, silica and titania. The latter membranes may act as intermediate supporting layers for micro-porous membranes. Transport descriptions for meso- and macro-porous ($Ø > 50$ nm) membranes are based on the concepts of Knudsen diffusion (gases only), viscous flow or Maxwell-Stephan (MS) multi-component transport (Dusty Gas Model for gasses). Transport in dense membranes is described by Onsager irreversible thermodynamics and often worked out in terms of concentration- and/or field-driven diffusion. The transport descriptions as mentioned are near-equilibrium approaches that incorporate semi-empirical expressions for the chemical potential (μ_I) of transporting species, *I*. The limited definition of state-of-the-art membranes justifies the use of ideal gas thermodynamics for gases, empirical Davies μ_I's for ions in liquids and Langmuir thermodynamics for surface adsorption and for most mobile species in 3-D lattices. Mobile electrons in cobaltates and metals form an exception to the latter, being better described as a Fermi liquid correlated electron system. Onsager cross-terms are seldom considered and are likely to be most relevant for molecular diffusion in gas mixtures *and* mixed electron-ion conductors; in both cases when different species have a significant energetic interaction. Differences in mobility of charged species may lead to the development of diffusion fields that can be incorporated in the chemical potential of that species. Single- and multi-component diffusion in liquids *and* in micro-porous and dense membranes can be described with chemical-, field- or MS diffusion coefficients. In solid state transport these can be related to mechanical mobilities for vacancy or interstitial mechanisms. Non-equilibrium correlation effects in diffusion can generally be ignored, except for the case of multi-component diffusion of species on a host lattice at high concentrations and with large differences in mobilities. Attempts to increase fluxes with thinner membranes have resulted in support transport resistances becoming comparable to membrane resistances. Complete descriptions of multi-component transport in supported membrane structures generally requires a numerical treatment with increasing importance of multi-scale methods. Those descriptions are needed to design fully optimized membrane structures and processes. The supports can be made at a reasonable cost by conventional ceramic pressing and extrusion techniques. Modern colloidal consolidation techniques enable very homogenous structures for accurate transport measurements and design of optimized graded porosity structures. For practical applications more attention must be paid to membrane adhesion, surface functionalization (hydrophobicity), thermochemical stability, mechanical and dimensional properties and sealing.

1. Introduction

Development of inorganic membranes started more than 50 years ago for separating $^{235}UF_6$ from $^{238}UF_6$. [1]. The membranes used for that purpose were thin layers of meso-porous γ-alumina on top of macro-porous ceramic supports, see Fig. 1. The separation is based on the fact that transport of the UF_6 gas molecules through the ~4 nm Ø pores in the γ-alumina layer is by Knudsen diffusion *and* that the theoretical Knudsen flux is inversely proportional to the square root of mass.

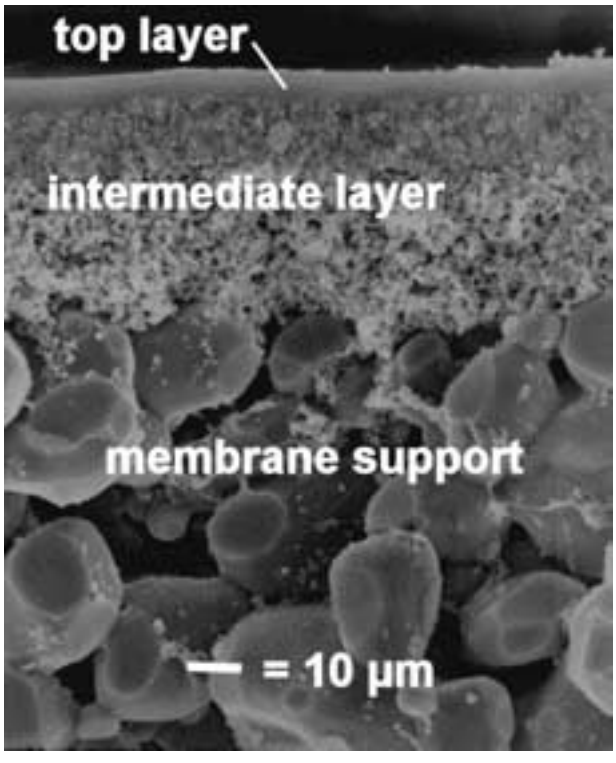

Figure 1 1990 State-of-the-art meso-porous γ-alumina membrane (top layer) on top of a macroporous α-Al_2O_3 "intermediate layer". The intermediate layer, in turn, is supported by a 2 mm thick macroporous membrane support. Reproduced with permission from [2].

Interest in inorganic membranes revived after 1980 with applications in liquid treatment and filtering particles and larger molecules. Attempts to broaden the application area in gas separation initially stalled because of the small Knudsen selectivity (being acceptable for the UF_6 process but not for lower value gasses). This situation changed with the advent of dense membrane materials such as Pd, $La_{1-x}Sr_xCoO_{3-\delta}$ and YSZ-noble metal dual phase composites *and* micro-porous membranes around 1990.

The ideal selectivity of dense membranes rests upon:

- transport of atomic or ionic (H and O) species by diffusion via available substitutional or interstitial vacancies,
- simultaneous transport of electronic charge carriers, by either normal metal electron-gas type conduction *or* by hopping on multivalent sites.

Ion- and electron transport in dense membranes can take place in a single homogeneous phase or in distinct phases in a bipercolative dual phase composite, both shown in Fig. 2.

Micro-porous membranes consist of zeolites, carbon or amorphous silica with connected pores of sub-nm dimension acting as an adsorption site for small molecules, see Fig. 3. The size and adsorption characteristics of the micro-pores lead to selectivities many orders of magnitude more than Knudsen combined with reasonably high fluxes. Application examples are isomer separation such as p-xylene from o-xylene, separation of H_2 or CO_2 from bigger molecules and H_2O from reaction mixtures.

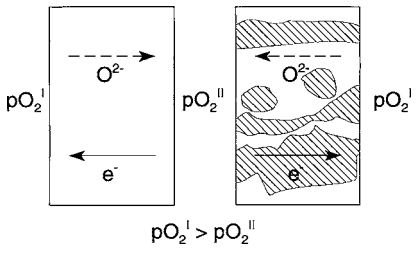

Figure 2 Schematic of net O_2 transport through dense homogeneous (left) and composite (right) membranes in response to a gradient in O_2 chemical potential, here expressed as p_{O_2}. Upon entering/exiting the solid structure, O_2 is converted into or formed from O^{2-} and electrons. These are transported simultaneously in a mixed-conducting single phase or a dual phase bipercolative composite. In both cases there is no connected meso- or macro-porosity. Transport may be governed by bulk- or surface-transfer limitations. Reproduced with permission from [2].

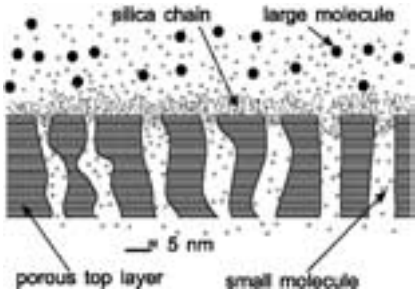

Figure 3 Schematic of separation and transport of small molecules by selective sorption in and diffusion through supported microporous amorphous silica membranes containing nearly linear silica polymers ("chains"). The (small) molecules in the (meso-)porous top layer are likely to have a mean free path length, larger than the pore diameter. In that case transport in the top layer can be described by Knudsen diffusion. Reproduced with permission from [2].

While meso-porous membranes have little interest for normal gas separation, beyond their role in supporting more selective membranes, they offer interesting perspectives for water purification. Supported γ-alumina membranes have demonstrated potential for water desalination and water softening. They have the possibility of elevated pressure gradients, high fluxes and rigorous cleaning conditions. Their selectivity rests upon the presence of space charge in the pore, induced by the adsorption of ions on the meso-pore surface, see Fig. 4.

1.1. Scope of this paper

The objective of the present paper is to present an overview of the field without going into deep detail and repeating existing overview papers for various inorganic membrane types. A recent overview of synthesis methods can be found in [2]. The paper will focus on complete supported membrane concepts and attempts to provide proper definitions and formally correct transport approximations. New approaches to synthesis of optimized ceramic membrane systems by particulate processing and random-packed structures, self-organization and micro-manufacturing techniques will be addressed on occasion.

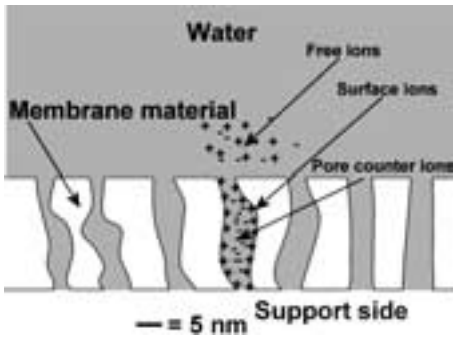

Figure 4 Spontaneous charging of the internal mesoporous membrane surface by preferential adsorption of positive ions leads to an excess of negative ions in the mobile pore liquid (to achieve overall charge neutralization). When a pressure gradient is applied across the membrane, the relative exclusion of positive mobile ions leads to an effective blocking of ions with respect to water molecules. Highly charged cations (Ca^{2+}) are blocked more effective than lower charged cations (Na^{+}), and vice versa for anions. Selective sorption of other (contaminant) ions may affect internal surface charging.

2. Morphology

2.1. Definitions

- *Agglomerate*: The second aggregation level in particle compacts.
- *Aggregation level*: Used for particle compacts to describe quasi-homogeneous groups of particles or packed structures that have similar dimensions. Level numbering increases with r_s^{disp} of the particles or structures. The particle compact itself presents the highest aggregation level.
- *Defects*: Generic term for point-, meso- and macro-defects as derived from the context.
- *Dense*: Descriptive term for a material with vacant sites, no larger than O(0.1 nm), corresponding to the size of substitutional or interstitial vacancies by which the mobile species are transported.
- *Domain*: The first aggregation level in particle compacts.
- *Fluidum*: Gas or liquid.
- *Graded structure*: Locally quasi-homogeneous support in which typical length scales, and possibly composition, vary monotonously and continuously in the direction, perpendicular to the membrane surface.
- *Isometric*: Used to describe particles with similar dimensions in all directions.
- *Point-defect*: Deviation from the ideal crystal structure with atomic dimensions.
- *Macro-defect*: Abrupt deviation from a quasi-homogeneous structure with typical dimension $r_{\text{def}} > 25$ nm.
- *Membrane*: Material with transport properties that result in relevant separations.
- *Meso-defect*: Same as macro-defect but with $1 < r_{\text{def}} < 25$ nm.
- *Micro-porous*: $r_p < 1$ nm. (This IUPAC definition deviates from common use in polymer membrane technology).
- *Meso-porous*: $1 < r_p < 25$ nm.
- *Macro-porous*: $r_p > 25$ nm.
- *Pinhole*: Fluidum meso- or macro-defect present over an entire layer thickness.
- *Primary particle*: Used for particle compacts to describe the smallest typical particle size.
- *Quasi-homogeneous*: Descriptive term for a material that appears homogeneous when spatially averaged over a length scale of $X^{\text{qh}} \approx 5r_s^{\text{disp}}$. This is the total thickness of three random-packed layers of particles with a typical radius r_s^{disp} from which the structures can be made.
- *Multi-layer structure*: Structure consisting of more than one distinguishable quasi-homogeneous layer.
- *Organized structure*: Solid structure with significant spatial correlation on length scales larger than X^{qh}.
- *Particle*: Apparently dense solid body with dimensions between 1 nm and 1 mm.
- *Random structure*: Solid structure without significant spatial correlation on length scales larger than X^{qh}.
- *Support*: Meso- and/or macro-porous structure providing mechanical rigidity to a (thin) membrane.
- *Supported membrane*: Layer of (thin) membrane material on a support.

2.2. Shape, scale and organization

Ceramic membranes, in particular dense perovskites and macroporous filters, have been made in many of the simple shapes that are possible with state-of-the-art ceramic pressing, extrusion, tape- and slip-casting techniques. Examples are thick disks and cylindrical and multi-bore tubes. Selective membranes, ranging from dense to meso-porous are also prepared as thin films on a meso- and/or macro-porous support with shapes as mentioned. While today many interesting membrane material concepts have been explored in depth, the presence of surface defects in the membrane support often leads to disappointing results, especially in permanent gas separation. An illustrative example is shown in Fig. 5 for thin dense $La_{0.5}Sr_{0.5}CoO_{3-\delta}$ membranes on a porous support of the same composition. In this text we will generally consider quasi-homogeneous structures and mention defects explicitly.

2.2.1. Relation between scale and flow

Resistance to flow, $n/\Delta p$, in meso- and macro-porous layers scales as:

$$n/\Delta p \propto \phi_{\text{p}}^{-1} r_{\text{p}}^{-\iota} \tau A^{-1} X \tag{1}$$

This resistance is established over X^{qh}. A supported membrane structure can be considered to be built up as a sequence of porous layers, u_k. Membranes and support layers are often made by deposition of a particle dispersion on an existing porous layer, $u_{k>0}$, followed by thermal processing or chemical conversion. If the dispersed particles have $r_{s,u_{k-1}}^{\text{disp}} < r_{p,u_k}$, one needs to observe the ratio, $r_{p,u_k}/r_{s,u_{k-1}}^{\text{disp}}$. Experimental results with deposition of γ-alumina membranes on α-Al_2O_3 supports indicated that $r_{p,u_k}/r_{s,u_{k-1}}^{\text{disp}}$ should be $<$ O (10) to

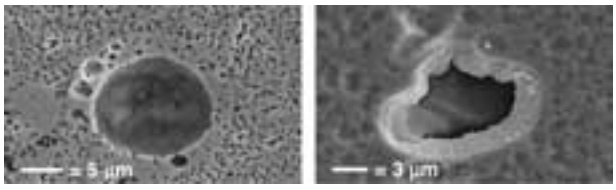

Figure 5 Porous support (left) made by colloidal filtration and sintering state-of-the-art $La_{0.5}Sr_{0.5}CoO_{3-\delta}$ powders. Chemical polishing of the support revealed several dense lumps and hollow spheres, formed in spray roasting. The hollow sphere surface-macro-defect resulted in a "pinhole" in the 10 μm thick $La_{0.5}Sr_{0.5}CoO_{3-\delta}$ membrane made by pulsed layer deposition (right). Such pinholes result in <100% selectivity for O_2 permeation. Reproduced from [3].

avoid excessive penetration of particles in the pores of the existing layer. The latter could lead to unacceptably increasing the transport resistance of the support structure: As an example a random particle layer $u_{k>1}$ is considered with $\phi_{p,k} = 0.4$ and filled over only one particle layer with much finer particles, also packing with $\phi_p = 0.4$. That one particle layer will have $\phi_p = 0.16$, $r_p = r_{p,k-1}$ and a thickness, equal to $2r_{s,k}$, much larger than $X^{qh}_{u_{k-1}} \approx 5r^{disp}_{s,u_{k-1}}$.

The top layer r_{p,u_1} must be sufficiently small to provide mechanical (bridging) support for the membrane layer and, possibly, to allow for a particulate membrane deposition process. Since flow resistance scales with $r_p^{-\iota}$, with $\iota \to 2$ for gasses at larger r_p-values [4], an optimized support structure will have subsequent layers u_k, with r_{p,u_k} increasing with k. The total number of support layers, k^{max}, is often restricted to two or three for practical or cost-price reasons. With such a restricted number it can be expected that $r_{p,u_k}/r^{disp}_{s,u_{k-1}}$ will be large and the $X_{u_{k<k^{max}}}$ will be kept close to their $X^{qh}_{u_k}$ in a compromise between pinhole risk and transport resistance. The classic example of Fig. 1 shows the thicknesses of the membrane top layer and the intermediate layer that are much larger than X^{qh} which is probably related to the state of the art in colloidal processing before 1990.

2.2.2. Thin layers

In the preparation of thin micro- and meso-porous layers, it is common practice to carry out the same layer deposition process two times or more. The rationale behind this is that occasional pinholes in the first layer will be bridged or filled during the second application with high statistical probability. Such pinholes are generally caused by gas bubbles or (airborne) particulate contamination. In addition, dense micro- and meso-porous films are often made with $X \gg X^{qh}$ to minimize the effect of low-density particle agglomerates or defects, as often occur in deposition of these films, see also Fig. 6. The fact that the total thickness of state-of-the-art membranes is currently much larger than what is actually needed may seriously hamper future applications. Avoiding particle agglomeration and defects in colloidal processing becomes increasingly difficult with particle sizes decreasing into the sub-10 nm range. Improved particle preparation, dispersion and deposition, and cleanliness during processing are likely to result in much thinner defect-free membrane structures.

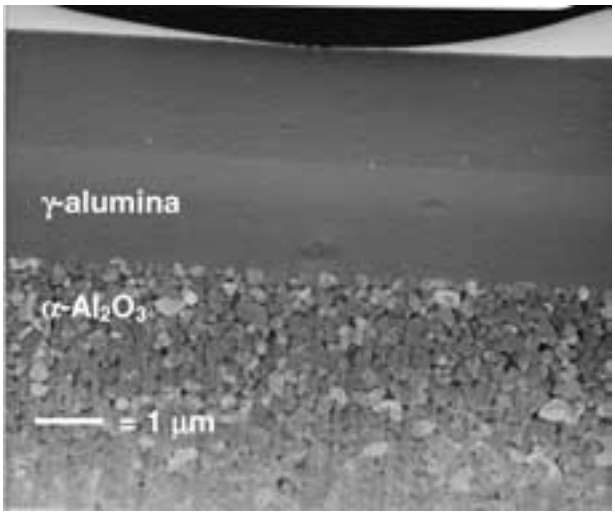

Figure 6 TEM FIB cross-section of macroporous α-Al_2O_3 support with two 1.5 μm thick γ-alumina layers. The γ-alumina layers show 100–300 nm low density areas (darker grey) due to the presence of agglomerates in the precursor γ-alumina. The presence of these areas makes that, up to now, fully functional γ-alumina membranes could never be made as a single layer and/or much thinner than 1 μm while $Z^{min}_{\gamma\text{-alumina}} \approx 50$ nm. The light-grey curved area (upper) is Pt, deposited to assist the FIB process.

2.2.3. Surfaces and interfaces

Fresh-formed porous layers generally have a near-surface morphology that deviates from the bulk structure. The surface that connects with an underlying support with much larger pores may exhibit a penetration structure as shown in Fig. 7. Surfaces that form from a liquid dispersion or interfaces with an effectively dense support may exhibit a slightly higher packing density.

Larger $r_{s,u_{k+1}}/r_{s,u_k}$ values may easily result in significant differences in properties and processing behavior between subsequent layers. This may lead to loss of

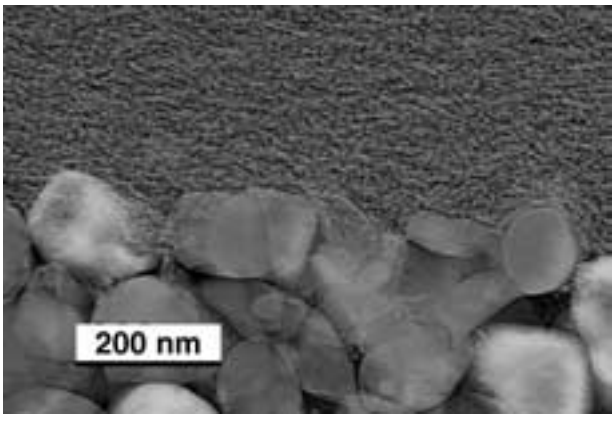

Figure 7 Enlargement of the α-Al_2O_3/γ-alumina interface as shown in Fig. 6. No special measures were taken to improve adhesion. Several microcracks between the γ-alumina (top) and the α-Al_2O_3 grains (bottom) are visible while γ-alumina (precursor) particle penetration was minimal and limited to the upper α-Al_2O_3 particle layer.

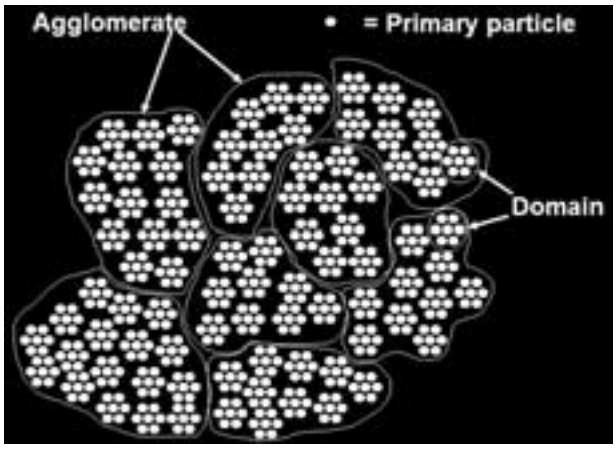

Figure 8 Schematic of a practical particle compact with 3 aggregation levels. Primary particles, for instance formed with $r_s^{disp} = O(5\ nm)$ from rapid precipitation reactions, may be present as organized domains. These domains can be random-packed into agglomerates. The agglomerates, in turn, can be packed to form the complete compacts. The number of aggregation levels can be <3 for carefully prepared compacts of similar isometric particles. In less homogeneous structures it can be >3, for instance if the agglomerates are combined into granules. Meso- and macro-defects may be present for the different size ranges, caused by impurities or imperfections in compaction processing.

interfacial integrity, directly after processing or during life time. Dense $X_m < 10\ \mu m$ films of $La_{0.5}Sr_{0.5}CoO_{3-\delta}$ on top of macroporous $La_{0.5}Sr_{0.5}CoO_{3-\delta}$ supports were found to develop spontaneous macro-porosity at high temperatures under the driving force of surface tension reduction [3]. This would not happen with a more gradual transition from dense to macro-porous. A recent example of a porous γ-alumina/α-Al_2O_3 interface, prepared by optimized colloidal processing that clearly illustrates possible problems is shown in Fig. 7. [1]

2.2.4. Random structures

Most practical random particle compacts contain a wide range of particle and pore sizes, as illustrated in Fig. 8. Since transport resistance scales with $r_p^{-\iota}$, it can be expected that all significant net flow will take place via connected porosity at the highest aggregation level. In the example of Fig. 8 that would be the inter-agglomerate porosity. As a consequence, in considering flow in porous layers, structure descriptions can be simplified to compacts with one aggregation level. However, the detailed compact structure still needs to be considered for transport by molecular diffusion, mechanical properties, conductivity, overall solid mass and thermo-chemical properties. Random dense packed particle compacts with one aggregation level will often provide the most favorable combination of properties. So, in this text we will assume that compact layers have one effective level of aggregation, unless indicated otherwise.

Layers with different scales require different synthesis and manufacturing methods:

- $r_p = O(0.2\ nm)$ for microporous amorphous silica requires template-assisted micro-pore formation, fully controlled by chemistry [6, 7]. The (organic) template is burnt-out by calcination.
- $r_p = O(1–300\ nm)$ for random-packed meso- and macro-porous structures requires colloidal-controlled assembly of particles initially dispersed in a liquid. The particle compacts obtain sufficient strength by a thermal (sintering) treatment that results in "necks" between the particles.
- $r_p > O(300\ nm)$ can no longer be achieved with colloidal assembly. Instead, conventional ceramic methods, involving binders, can be used. Such methods are also used for the smaller size range but in that case lead to poor stacking homogeneity. For particles with $r_s^{disp} > 10\ \mu m$, normal thermal processing may not result in sufficient neck formation and the particles may need to be connected with inorganic adhesives such as low-melting glass or aqueous phosphate solutions [8].

2.2.5. Organized structures

The tortuosity contribution to the resistance (1) is $\tau \approx 3$ for random packed structures. In more organized structures, the resistance can be much less with ultimately $\tau = 1$ for straight pores. Assuming mono-sized pores and no strength constraints, flat macro-porous structures can be (top-down) micro-manufactured with $\phi_p < 0.9$, more than normally achieved in random particle packing. This offers additional perspectives for reducing resistance. An example of a micro-manufactured "microsieve" with $r_p = 150\ nm$ and $\phi_p = 0.2$ is shown in Fig. 9. Organized structures can be made at all relevant length scales. "Bottom-up" methods make use of chemistry and physics, intrinsic to the system; (micro-) manufacturing ("top-down") methods start with homogeneous materials in which detailed structures are realized by chemical, physical or mechanical machining

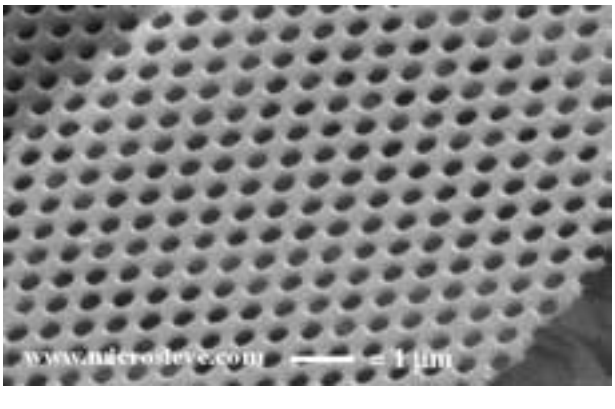

Figure 9 Micro-manufactured organized macro-porous sheet (microsieve) made by laser interference lithograpy in a Low Pressure Chemical Vapour Deposition (LPCVD) 'stress free' silicon-rich siliconnitride membrane [9]. The membrane is supported by a silicon wafer, in which large rectangular perforations of 100 μm by 2000 μm have been etched with KOH. The pore Ø, here 300 nm, can be between between 50 nm and 10 μm and the thickness of the micro-sieve between 0.1 and 2 μm. The pressure strength of these sieves is typically 4-5 bar. (Kindly supplied by Dr. C.J.M. van Rijn of AQUAMARIJN Micro Filtration B.V.).

[1] Interlayer adhesion can be improved with inorganic adhesives while high-temperature stability of porous structures can be improved by surface-active ions [5] or by dispersing a non-reactive second phase.

methods.[2] Bottom-up and top-down methods meet in the mesoscopic size-range. For organized structures, different scales require various synthesis and manufacturing methods:

- $r_{p,m}$ = O(0.1 nm) in dense membrane materials that form by crystallization and chemical deposition [3] or thermal processing of particle compacts [10]. They:
  - may exhibit ordering of substitutional vacancies over O(>10 nm) length scales such as occurs frequently in perovskite-based structures [11]. This increases τ because the ordered regions act as a dispersed inert phase in the main phase,
  - often have a polycrystalline structure with r_{grain} = O(1 μm). This may introduce grain boundary cross-over transport impediment and orientational tortuosity for (occasional) non-cubic lattice symmetries,
  - may be one of the components in a dual phase composite structure [12]. Such structures are often made by thermal processing of a random particle compact. In that case the composite will consist of two percolative and tortuous structures with $\tau > 1$, typically O(3).[3]
- r_p = 0.2–1 nm in zeolite membrane materials that form by template-assisted crystallization and into membranes by in-situ growth: directly on a support *or* in the connected pores of particle compacts. The most popular zeolite in membrane technology is MFI, followed on a distance by SOD [13]. They:
  - may have connected micro-pores that are part of the regular zeolite crystal structure and that are either straight or "zig-zag" (the organized variant of tortuosity; MFI has both straight and zig-zag pores),
  - often have a polycrystalline structure with r_{grain} = 0.1–1 μm. This may introduce grain boundary cross-over transport impediment and orientational tortuosity for (very common) non-cubic lattice symmetries (as in MFI),
  - may be ordered into an oriented structure [14]. For cubic structures (as SOD) this offers the only advantage of the absence of grain boundaries. For non-cubic structures this offers the additional advantage of minimizing transport resistance if the micro-pores, with the most favorable transport properties, are oriented perpendicular to the membrane.
- r_p = 1–15 nm in organized mesoporous materials. These materials can be formed from surfactant-assisted self-organized meso-structures [15, 16]. Most popular are many different forms of organized meso-porous silica, and such materials were recently used to support thin micro-porous membranes [17]. There are no well-documented examples of long-range colloidal crystallization for this size range. The largest sizes in this range may overlap with what can be achieved with advanced (top-down) micro-manufacturing methods.
- $r_p > 25$ nm can be achieved routinely in state-of-the art micro-manufacturing as shown in Fig. 9. Similar structures have been realized starting with 2D-colloidal organization of mono-sized template spheres on an interface. Interfacial polymerization between the spheres [18], followed by dissolving them leads to a highly permeable polymer sieve with some positional disorder. 3D-colloidal crystallization of mono-sized spheres generally leads to close-packed structures with $\phi_p = 0.28$ and poor permeability. Moreover, such structures easily form macro-defect packing faults. For the $r_p > 1$ μm sizes range, more traditional manufacturing methods can be used to realize highly permeable sieve structures.

2.2.6. Optimized structures

Assuming quasi-homogeneous structures and that ϕ_p and τ are about the same for all support layers, one may expect that mechanical strength of the individual layers decreases with r_p. As a consequence a complete optimization of multilayer support structure properties, including strength may result in $X_{u_l}^{opt} > X_{u_l}^{qh}$. In many membrane processes there is a significant difference between the membrane-side total pressure, p^m, and the support-side total pressure, p^u. In these processes, using the same assumptions for ϕ_p and τ, local stress gradients, $\nabla\sigma_{xx}$, will develop in the support that scale with $r_{p,u_k}^{-\iota}$. The largest $\nabla\sigma_{xx}$ will generally be in the membrane. This has the consequence that in a support structure that monotonously coarsens with x, σ_{xx} will be predominantly tensile if $p^u > p^m$ and predominantly compressive if $p^u < p^m$. For brittle, full ceramic structures the latter is preferred which gives additional arguments for a support structure that coarsens monotonously with x.

The decision of what supported membrane structure will eventually be chosen for a given application will depend on:

- The availability of design optimization tools that involve:
  - accurate predictions of the strength of a complete structure,
  - accurate life-time and cost-price predictions,
  - fundamental transport parameters for various components of the supported membrane structure and fully integrated and formally correct transport descriptions for the complete structure. The availability of accurate transport parameters, in turn, depends on the availability of well-defined materials and structures.
- The availability of synthesis and manufacturing methods for all relevant size ranges.

[2] In the membrane community such structures are known as "track-etched membranes".

[3] It would be interesting to avoid this tortuosity with micro-manufactured structures. However, the fact that charge carriers are in different phases makes that here also the size matters; the smaller the better.

For $r_p < 1$ nm, bottom-up methods may be the only ones available and generally at a reasonable cost. The only problem is that we are limited to what nature has to offer. For $1 < r_p < 15$ nm, use of surfactant-assisted self-organization structures may eventually be the best choice. Possible drawbacks are the occurrence of meso-defects due to stacking faults and the fact that, currently, the dominant material is silica which may not be a suitable composition. For $15 < r_p < 300$ nm random-packed structures by colloidal assembly are probably most viable. But, in particular, for the larger size ranges, micro-manufacturing methods are likely to become more and more competitive. In relation to this, it is noteworthy that the largest relevant size: that of the complete supported structure is always a manufactured shape (disk, tube, hollow fiber, multi-bore).

Taking into account the need for:

- a fine porous surface at the membrane side,
- a narrow effective pore size distribution in the plane, parallel to the membrane,
- a structure that connects to the membrane surface but monotonously coarsens with x,
- absence of penetration of fine particles in the pores between coarser particles,
- absence of clear interfaces between layers with largely different r_s,

One easily arrives at the conclusion that the ultimately optimized membrane support structure, will be a *graded* structure in which r_p is a continuous and monotonously increasing function of x. In this structure $O(r_p)$ may range from 1 nm to 1 mm and it is unclear whether affordable processes to realize this complete range will ever become fully available. It will be a challenge to make graded structures with bottom-up methods [19] and it will be difficult but not impossible to realize them with micro-manufacturing techniques. Fig. 10 shows how such a structure could look.

The future supported inorganic membrane structure, fully optimized for cost, is likely to be a high-definition, high-performance device with a small projected surface area and high permeability and durability. It may have membrane and support layers by crystallization or self-organization for the smallest size range. Both organized and random-packed structures may be the choice for meso-porous layers. The smaller macro-pore range may be realized best with a random-packed structure and shaping in the biggest size ranges will always be by top-down manufacturing. Complicated top-down ceramic structures are likely to be most affordable when the actual forming takes place with a highly fluid polymer-ceramic particle mixture [20, 21], followed by solidification and thermal processing.

In optimized structures we may be able to identify systematically: a transition from bottom-up organized to random-packed *and* a transition from random-packed to top-down organized. Those transitions are preferably made without too abrupt changes while at least part of the structure can be of the graded type. The first transition is expected to move to bigger size ranges while the second is expected to move to the smaller sizes. Due to this, random-packed structures may eventually disappear and the physics and chemistry of bottom-up assemblies will connect seamless with chemical and mechanical engineering of top-down structures.

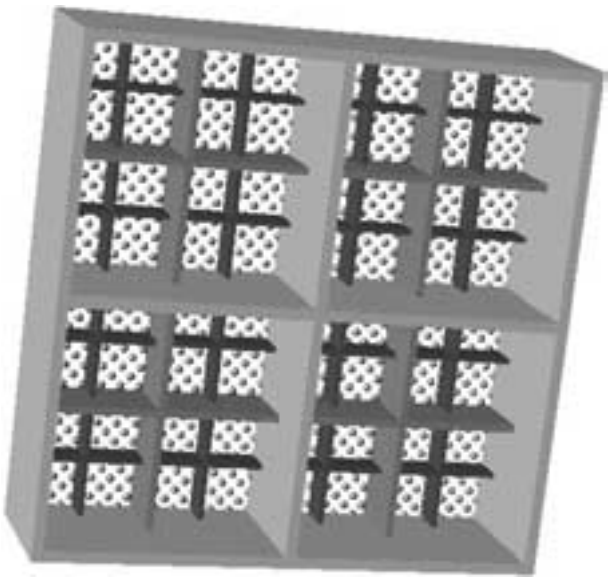

Figure 10 Envisioned highly permeable graded organized structure with 3 different pore sizes. To span a complete pore-size-range of 1 nm to 1 mm with a similar structure would require 20 different pore sizes. The square geometry is not optimum for flow; structures with cylindrical elements or rounded corners, to be defined yet may provide a better optimum.

3. Transport properties

3.1. Definitions

- *Correlated transport process*: Process in which subsequent steps are influenced by history. The most well-known example is quasi-equilibrium vacancy diffusion on a lattice with $\theta \to 1$. One particular species that just made a diffusion hop leaves behind a vacancy on its original location. Since that location becomes vacant with 100% certainty, not the case for the other neighboring sites, the probability that the species moves back to its original location is larger than what can be expected from statistical availability.
- *Correlated electron system*: Electron band structure in which the position of individual electron states depends on the amount of band electrons per structural unit R.
- *Fermi level*: Highest occupied level in an (electron) band structure at $T = 0$. This (thermodynamic) definition deviates from what is commonly accepted in the semiconductor community that uses the Fermi level to indicate μ_e.
- *Formally correct*: Description that can be simple but internally consistent for both equilibrium and transport descriptions. For instance in the ideal Langmuir lattice: b^0 must be independent of θ.
- *Ideal system*: Refers to species, l, in an ideal gas or diluted in a liquid, such that (18) is valid and $b_l = b_l^0$.

- *Ideal Langmuir lattice*: Lattice on which species, l, can be randomly distributed with h_l and s_l^0, independent of l.
- *Quasi-binary*: System of mobile species and vacancies in which the latter can be treated, from thermodynamic point of view, as normal mass species.
- *Quasi-equilibrium*: Refers to a real equilibrium system in which an inhomogeneously distributed part of the mobile species are labeled either physically or logically.
- *Unconditional*: Imaginary condition for the mobility of species in which all neighboring sites with similar physical properties are immediately available for a transport step.

3.2. Onsager equations

The objective in exploratory membrane research is often realizing a material with transport properties for binary separation. This objective can be translated into the phenomenological Onsager equations of irreversible thermodynamics for mobile species l_1 and l_2, present in the membrane structure, m:

$$j_{l_1} = -L'_{l_1,l_1}\nabla\tilde{\mu}_l - L'_{l_1,l_2}\nabla\tilde{\mu}_m - L'_{l_1,\mathrm{m}}\nabla\tilde{\mu}_\mathrm{m} \quad (2)$$

$$j_{l_2} = -L'_{l_1,l_2}\nabla\tilde{\mu}_{l_1} - L'_{l_2,l_2}\nabla\tilde{\mu}_{l_2} - L'_{l_2,\mathrm{m}}\nabla\tilde{\mu}_\mathrm{m} \quad (3)$$

$$j_\mathrm{m} = -L'_{l_1,\mathrm{m}}\nabla\tilde{\mu}_{l_1} - L'_{l_2,\mathrm{m}}\nabla\tilde{\mu}_{l_2} - L'_{\mathrm{m},\mathrm{m}}\nabla\tilde{\mu}_\mathrm{m} \quad (4)$$

In which $\nabla\tilde{\mu} = \frac{d\tilde{\mu}}{dx}$ and the Onsager symmetry relations were applied.

Examples are:

- Separation of O_2 from air with dense perovskite membranes and 100% selectivity in which the mobile species are oxygen ions and electrons (or holes).
- Separation of H_2 from H_2/CO_2 mixtures with microporous membranes and <100% selectivity in which the mobile species are molecular H_2 and CO_2.

The transport coefficients in (2)–(4) have been provided with primes ($'$) to distinguish them from the simpler expressions (6) in which the membrane is made "invisible" by application of the Gibbs-Duhem relation:

$$c_{l_1}d\mu_{l_1} + c_{l_2}d\mu_{l_2} + c_\mathrm{m}d\mu_\mathrm{m} = 0 \quad (5)$$

Obtaining $d\mu_\mathrm{m}$ from (5), followed by substitution in (2) and (3), and rearrangement lead to the regular Onsager equations for a binary mixture:

$$j_{l_1} = -L_{l_1,l_1}\nabla\tilde{\mu}_{l_1} - L_{l_1,l_2}\nabla\tilde{\mu}_{l_2} \quad \text{and}$$
$$j_{l_2} = -L_{l_1,l_2}\nabla\tilde{\mu}_{l_1} - L_{l_2,l_2}\nabla\tilde{\mu}_{l_2} \quad (6)$$

3.2.1. Cross-coefficients

For the dense membranes, the cross-coefficient L_{l_1,l_2} depends on the extent of interaction between the ionic and electronic species. It can be ignored in (fuel cell) electrolytes in which ion transport prevails over electron transport. It can be made zero in mixed-conducting dense membranes by a proper choice of the effective charge of the transported ions [22]. The diffusion field that develops in systems with more mobile charge carriers may be incorporated by the $q\Phi$ term in $\tilde{\mu}$ and does not contribute to a cross-coefficient. For microporous molecular transport, L_{l_1,l_2}, can be assumed to be zero to first order approximation [23]. In Knudsen separation L_{l_1,l_2} is zero by nature of the transport mechanism (the molecules only meet the pore walls and not each other). So for many relevant cases the transport equations can be simplified to:

$$j_{l_1} = -L_{l_1}\nabla\tilde{\mu}_{l_1} \quad \text{and} \quad j_{l_2} = -L_{l_2}\nabla\tilde{\mu}_{l_2} \quad (7)$$

3.2.2. Diagonal Onsager equations and mechanical mobility

Having the Onsager equations in the diagonal form allows us to focus on expressions for a single mobile species, l, *and* to exploit the concept of *mechanical mobility*, b_l. In a fully dissipative transport process, b_l provides a connection between the time-averaged stationary velocity, $\bar{v}_l$ and the (thermodynamic) driving force, $\bar{F}_l$, acting on the mobile species l:

$$\bar{v}_l = b_l\bar{F}_l \quad (8)$$

Substitution of $\bar{v}_l = j_l/c_l$ and $\bar{F}_l = -\nabla\tilde{\mu}_l$ leads to:

$$j_l = -b_l c_l \nabla\tilde{\mu}_l \quad (9)$$

This identifies the phenomenological L_l as $b_l c_l$ which provides:

- a useful tool in creating systematics in diffusion coefficient definitions and notations,
- an opportunity to incorporate microscopic information in expressions for b.

The first aspect will be worked out further in Section 3.4. An example of the second aspect is an expression for the uncorrelated mechanical mobility in chemical diffusion via a vacancy mechanism:

$$b_l = \tilde{f}_{l,L}b_l^0(1-\theta) \quad (10)$$

This expression is based on the assumption that the unconditional mobility, b_l^0, is reduced by a factor $(1-\theta)$. This is due to the fact that, on the average, a fraction $(1-\theta)$ of the neighboring sites will be occupied by other species and hence not be available for hopping diffusion. In single component diffusion $\theta = \theta_l$. In multi-component diffusion, $\theta = \sum_{l=1}^{l=l^\mathrm{max}}\theta_l$, showing that b_l can depend on the concentration of all mobile species. The non-equilibrium correlation factor, $\tilde{f}_{l,L}$, is likely to depend on θ, $\nabla\theta$, b of all mobile species *and* the topology of all sites on lattice, L, that are available for mobile species. Numerical values can be obtained with Monte-Carlo simulations of multi-component lattice diffusion. For many practical

situations $\tilde{f}_{l,L}$ appears to be very close to unity. An important exception is the case of two-component diffusion on a micro-pore lattice with one slow and one fast component [24]. Quantitative expressions for $\tilde{f}_{l,L}$ and relations with other quantities need to be better explored and investigated. In the remainder of this document we will assume that $\tilde{f}_{l,L} = 1$, unless otherwise indicated.

In stationary membrane transport, j_l is constant with x, while c_l can be expected to vary with x.[4] Likewise b_l is expected to vary with x through its dependence on θ (or c) of all mobile species. The value of $\nabla\tilde{\mu}_l$ depends largely on boundary conditions set by chemical potentials of the mobile species at the feed and permeate side and membrane thickness, X. In detail, $\nabla\tilde{\mu}_l$ wuld depend on x such as to make the stationary $b_l c_l \nabla\tilde{\mu}_l$ products constant. The challenge of finding an interesting membrane material in an exploratory study comes down to finding $b_l c_l$ products for specific cases that result in interesting separation (or electrolyte) behavior.

Experimental bc values for dense membranes can be derived from gas-solid equilibrium measurements (for c) and targeted (electric) transport measurements (for b). Likewise values for microporous membranes can be obtained from adsorption equilibria (for c) and nuclear resonance mobility measurements (for b). The use of such measurements can be affected by the lack of bulk quantities of materials with exactly the intrinsic properties of the membrane material. This often has the consequence that the materials have to be made as real (supported) membranes to study their actual permeation behavior [25]. In addition, the translation of thermodynamic and mobility data of bulk materials to intrinsic membrane transport data relies on detailed microscopic insights and accurate analyses that only recently started to become available [26]. The remainder of this section provides a significant part of the conceptual framework for such an analysis.

3.3. Equilibrium thermodynamics

As indicated in Section 3.2, expressions for transport in membrane materials can be formulated in terms of $\nabla\tilde{\mu}$. This is the simplest assumption that can be made for transport in a non-equilibrium system if one realizes that in equilibrium systems, in which there is no net transport of matter, all $\nabla\tilde{\mu} = 0$. In any case it is very important to use expressions for μ_l that are formally correct and consistent with other assumptions made for the transport equations.[5]

3.3.1. Ideal Langmuir lattice

The state of the art in synthesis of supported inorganic membrane structures justifies the use of simple approximations. As an example we discuss first the chemical potential of species on an ideal Langmuir lattice which provides a good approximation for the following cases:

- Distribution of vacancies on regular oxygen sites in dense (perovskite) membranes.
- Distribution of localized but still mobile electrons and holes (small polarons) on multi-valent cation sites in dense membranes. (As shown in [27], this description is not appropriate for cobaltates.)
- Distribution of atomic hydrogen on interstitial sites in Pd.[6]
- Sorption of atomic and molecular species on a 3D-connected micro-pore lattice as present in zeolites and envisioned to be present in micro-porous amorphous silica.
- Adsorption of ions, atoms and molecules on surfaces that provide a regular 2D lattice of adsorption sites. This approach is useful for adsorption from the gas phase and for adsorption of ions from a polar (aqueous) solution.

The μ for species on a Langmuir lattice can be written as:

$$\mu_l = \mu_l^0 + \mathrm{k_B}T \ln\left(\frac{\theta_l}{1-\theta}\right) \tag{11}$$

$$\mu_l^0 = h_l - T s_l^0 \tag{12}$$

In which h_l and s_l^0 are independent of θ and slightly T-dependent, due to vibrational and possibly rotational contributions.

The numerator in (11) represents the relative occupancy (concentration) of the actual species while the denominator represents the relative occupancy (concentration) of vacancies. In the area of defect-chemistry similar terms are often assigned to members of pairs of conjugated defect species. This enables the use of Kröger-Vink symbols to write normal chemical reaction equations with individual defect species under certain conditions. An example is the oxidation reaction of gaseous O_2 with sub-stoichiometric $Fe_2O_{3-\delta}$, written in Kröger-Vink notation for the solid species:

$$4\mathrm{Fe}'_{\mathrm{Fe}} + 2\mathrm{V}_{\mathrm{O}}^{\cdot\cdot} + \mathrm{O_2(g)} \rightleftarrows 4\mathrm{Fe_{Fe}} + 2\mathrm{O_O} \tag{13}$$

Both $\mathrm{V}_{\mathrm{O}}^{\cdot\cdot}$, $\mathrm{O_O}$ and $\mathrm{Fe}'_{\mathrm{Fe}}$, $\mathrm{Fe_{Fe}}$ form conjugate pairs and ideal Langmuir thermodynamics are often assumed for the associated real species. The chemical potential of an O^{2-} ion formed on the oxygen sub-lattice of Fe_2O_3 can be written as:

$$\mu_{\mathrm{O}^{2-}} = \mu^0_{\mathrm{O}^{2-}} + \mathrm{k_B}T \ln\left(\frac{\theta_{\mathrm{O}^{2-}}}{1-\theta_{\mathrm{O}^{2-}}}\right) \tag{14}$$

This complete potential can be split up into two half potentials as:

$$\mu_{\mathrm{O}^{2-}} = \mu_{\mathrm{O_O}} - \mu_{\mathrm{V}_{\mathrm{O}}^{\cdot\cdot}} \tag{15}$$

[4] Not in electrolytes.

[5] Systems largely out of equilibrium may require a non-linear irreversible thermodynamics approach but that has not yet been explored well for membranes. This may become interesting in case membranes become available with much higher fluxes than what is currently available.

[6] The Pd metal electronic structure may be affected though.

In which:

$$\mu_{O_O} = \mu^0_{O_O} + k_B T \ln \theta_{O_O} \quad (16)$$

$$\mu_{V_O^{\cdot\cdot}} = \mu^0_{V_O^{\cdot\cdot}} + k_B T \ln \left(1 - \theta_{O_O}\right) = \mu^0_{V_O^{\cdot\cdot}} + k_B T \ln \theta_{V_O^{\cdot\cdot}} \quad (17)^7$$

The use of Kröger-Vink symbols and their "half-potentials" will generally lead to correct results in equilibrium relations because conjugate pairs are always kept together in compliance with the Kröger-Vink conditions for solid state reaction equilibria. The reaction equation $O^{2-}(ext) + V_O^{\cdot\cdot} \rightleftarrows O_O$ leads to the correct expression (15) when potentials are substituted for species. Use of the half-potentials may occasionally lead to correct results in irreversible thermodynamics transport treatments, but not as a rule. In transport considerations the members of conjugate pairs are no longer required to occur together such as to justify the use of half potentials. The use of transport expressions and quantities with Kröger-Vink species should be avoided. As an alternative the species could be named:

- Simply as O^{2-} and $V_{O^{2-}}$ in the example.
- By using the, now somewhat obsolete and not so easy to understand, Schottky notation [28].
- By using the notation of [22], that is based on the Kröger-Vink notation.

Finding a simple and formally correct notation is a subject of future studies.

When $\theta \to 0$, (11) simplifies to:

$$\mu_l = \mu^0_l + k_B T \ln(\theta_l) = \mu^0_l + k_B T \ln\left(\frac{c_l}{c^{tot}}\right) \quad (18)$$

In which c^{tot} is the total number of available sites on the lattice per unit volume.

3.3.2. Treatment of vacancies

Treatment of vacancies in irreversible thermodynamics-based transport equations has been a source of confusion in recent literature. It is generally possible to avoid complications by writing all transport equations in terms of real mass species. We pay attention to the subject because it may add to understanding and new insights.

In the previous section we already pointed out that the use of Kröger-Vink vacancies and half-potentials should be avoided in transport equations. From the formal thermodynamic point of view there is the concern that no μ can be assigned to a mass-less species that can be spontaneously created or annihilated. This is well-known for lattice vacancies in pure metals that can reach a certain equilibrium c at a given T, because they can be created or annihilated at boundaries and dislocations. The μ of a species in a phase is defined as the change of free enthalpy/energy of that phase when one such species is added or deducted. Adding a vacancy to a pure metal would initially increase the vacancy c, followed by re-equilibration to the equilibrium c, In the end neither the free enthalpy nor anything else has changed. More in general, the formation of vacancies in solid elements and compounds built-up from atomic or molecular units, R, can be written as:

$$0 \rightleftarrows V_R \quad (19)$$

This equation cannot be converted into an isomorphic chemical equilibrium equation by substitution of chemical potentials for species. Representative examples of R are Pd, $La_{0.5}Sr_{0.5}CoO_{3-\delta}$ and SiO_2 (silicalite zeolite). However, it is possible to assign a chemical potential to vacancies in situations where the total number of lattice sites is fixed and the number of vacancies is just the balance of the number of occupied sites. In that case, the vacancies can be treated similar, in thermodynamic expressions, to any other mass species that would occupy the same sites. In other words, in a binary system, a fraction θ_{l_1} of the sites may be occupied by l_1 while the balance $(1 - \theta_{l_1}) = \theta_{l_2}$ is occupied by l_2. With a fixed number of sites, either l_1 or l_2 can be vacancies in a quasi-binary system without any noticeable consequences for model-based thermodynamic expressions for both. [8] Examples of situations with a fixed number of sites are as follows:

- Site-sublattices such as:
  - the interstitial vacancy sub-lattice in Pd,
  - the oxygen sub-lattice in perovskites,
  - the micro-pore lattice in zeolites.

  In those cases the number of sub-lattice sites is fixed because the total number of R units is fixed.
- The interior of large perfect crystals (without dislocations, grain-boundaries and pores) in which the vacancy exchange with external surfaces is irrelevant. The lattice can in this case be thought of as a sub-lattice of an imaginary structure.

The massless vacancies in these lattices can be assigned model-based thermodynamic potentials as if they were normal mass species. In case the Gibbs-Duhem relation is applied to remove the membrane from transport equations as (2)–(4) to result in (6), any vacancies that occur as mobile species can be thought of as representing the (immobile) membrane mass species or the imaginary structure, creating the lattice. Such vacancies could be identified as "Gibbs-Duhem vacancies". It is easy to draw a 1:1 thermodynamic parallel between atomic species and vacancies on a fixed lattice

[7] The split-up of $\mu^0_{O^{2-}}$ into $\mu^0_{O_O} - \mu^0_{V_O^{\cdot\cdot}}$ can be done quite arbitrarily. The value of $\mu^0_{O^{2-}}$ can also be taken arbitrarily as part of the overall reaction $\mu^0_{O_X}$ of (13) or thought to be formed from an imaginary entropy-less O^{2-} reservoir. Further discussion of these thermodynamic "gauging" aspects are beyond the scope of this paper.

[8] The fact that vacancies l_2 may actually be needed to provide mobility for l_1 is no concern here. That only affects transport via the mobility considerations.

and localized electrons and holes on a fixed lattice of multi-valent ions. The complete chemical potential for vacancies, $\widehat{\mathrm{V}}$, on an ideal Langmuir lattice, to be used in irreversible thermodynamic transport expressions is:

$$\mu_{\widehat{\mathrm{V}}} = \mu^0_{\widehat{\mathrm{V}}} + \mathrm{k_B}T \ln\left(\frac{1-\theta}{\theta}\right) \tag{20}$$

3.3.3. Ions in solution

Species dissolved in a liquid can also be considered as being distributed over a regular (non-stationary) lattice. For ideal solutions, (18) may be used. For ions in solution, a correction for electrostatic interactions is generally needed. For the purpose of inorganic membrane separations with ionic solutions the Davies' expression [29] can be used:

$$-\log(\gamma_l) = 0.51 z_l^2 \left(\frac{\sqrt{I^{\mathrm{c}}}}{1+\sqrt{I^{\mathrm{c}}}} - 0.2 I^{\mathrm{c}}\right) \tag{21}$$

In which:

$$I^{\mathrm{c}} = \frac{1}{2}\sum_{l=1}^{l=l^{\max}} \frac{c_l z_l^2}{c^0} \tag{22}$$

And γ_l is used for:

$$\mu_l = \mu_l^0 + \mathrm{R}T \ln\left(\frac{\gamma_l c_l}{c^0}\right) \tag{23}$$

3.3.4. Ideal gas species

For membrane equilibrium and transport equations, species in the gaseous state, are often described assuming ideal gas behavior. The chemical potential for such species, l, is generally written as:

$$\begin{aligned}\mu_{l,\mathrm{g}} &= \mu^0_{l,\mathrm{g}} + \mathrm{k_B}T \ln\left(\frac{p_l}{p^0}\right) \\ &= \mu^0_{l,\mathrm{g}} + \mathrm{k_B}T \ln\left(\frac{c_l}{c^0}\right)\end{aligned} \tag{24}$$

In which $c^0 = p^0/\mathrm{R}T$. This expression can also be used for free electrons and holes that behave, thermodynamically, as an ideal gas. Examples are free electrons and holes near the band edges of a normal, lightly doped semiconductor. For mono-atomic and electronic ideal gases:

$$h_{\mathrm{g}} = \pm\frac{3}{2}\mathrm{k_B}T \quad \text{(with the minus sign for holes)} \tag{25}$$

$$s^0_{\mathrm{g}} = \mathrm{k_B} \ln\left[\frac{g\,(2\pi m \mathrm{k_B}T)^{3/2}}{\mathrm{h}^3 C^0}\right] \tag{26}$$

In which g can be an electronic state multiplicity, m is the thermal effective mass for electrons and holes and $C^0 = c^0 \times N_{\mathrm{Av}}$. For multi-atomic gases, rotational and vibrational terms can be added to (25) and (26). Both (25) and (26) show a clear T-dependence but one that is weak as compared to normal Arrhenius-type T-dependance. When combined into $\mu^0_g = h_g - Ts^0_{\mathrm{g}}$, the T-dependence of of h_{g} and Ts^0_{g} cancel each other partially. This makes (24) of particular practical use. However, as shown in [30], micro-porous membrane permeation processes with $\theta \to 0$ may show a very weak overall T-dependence in which the use of more detailed expressions for the solid state and the gas phase may be justified.

3.3.5. Relation between ideal and $\theta \to 0$ Langmuir systems

While the ideal gas μ results from a distribution of species over abundant kinetic states, the Langmuir μ results from a distribution of species over positions. Relation (18) for μ on a Langmuir lattice with $\theta \to 0$ bears a remarkable similarity with (23) and the c-version of (24). The differences are in detailed expressions for μ^0. Since many species in inorganic membrane technology fulfill roughly the underlying assumptions for either one of these expressions, commonly used equations tend to lead towards (23). However, the introduction of activity coefficients, γ, should be done with caution and not until an expression for μ is obtained, consistent with the most basic characteristics of the system. When considering higher concentrations in Langmuir systems, the $(1-\theta)$ in the denominator should be the first "correction" to the θ_l term. The activity coefficient γ should not be used as a mathematical transformation of μ, but instead be reserved for the final, semi-empirical correction as in (21)–(23). [9]

3.3.6. Electron thermodynamics

Ideal gas electrons and holes, as occur in lightly doped semiconductor, have a chemical potential (24). Practical use for membranes is in calculating parasitic permeation in electrolytes, caused by minimal mixed conduction with mobile electrons in the conduction band.

Small polaron electrons and holes can be considered as localized but still mobile, and can be treated in the simplest approximation as being distributed in a quasi-binary system on a Langmuir lattice. The system of $\mathrm{Fe}'_{\mathrm{Fe}}$ and $\mathrm{Fe}_{\mathrm{Fe}}$ species on the Fe sub-lattice of $\mathrm{Fe_2O_3}$ in (13) can also be considered as a system of either:

- Electrons ($\mathrm{Fe}'_{\mathrm{Fe}}$) and "electron vacancies" ($\mathrm{Fe}_{\mathrm{Fe}}$, not to be confused with holes) on a $\mathrm{Fe}_{\mathrm{Fe}}$ system.
- Holes ($\mathrm{Fe}_{\mathrm{Fe}}$) and "hole vacancies" ($\mathrm{Fe}'_{\mathrm{Fe}}$, not to be confused with electrons) on a $\mathrm{Fe}'_{\mathrm{Fe}}$ system.

In $\mathrm{Fe_2O_{3-\delta}}$ with $\delta \to 0$, "$\mathrm{Fe}'_{\mathrm{Fe}}$ "electrons will be more mobile than "$\mathrm{Fe}_{\mathrm{Fe}}$" holes, with nearly all the neighboring sites being $\mathrm{Fe}_{\mathrm{Fe}}$ and available for electron hopping. It is for this reason that the mobile charge carriers will be identified as "electrons" but

[9] The μ of species in a band of kinetic states, narrow with respect to $\mathrm{k_B}T$, shows striking similarities with (11). This is left as an exercise for the reader.

this choice is rather arbitrary. The μ for the electrons and holes, distributed and localized on a Langmuir lattice at low concentrations, appears as the *c*-version of (24) as was the case for their ideal gas counterparts. Again, there are significant differences in the detailed expressions for μ^0. The ideal Langmuir description for mobile electronic charge carriers can be used as a simple but adequate approximation for many dense membrane transition metal oxides (except for the cobaltates).

For mobile electrons, e, in normal metals (24) definitely does not apply. Those "metal electrons" are assumed to be present in a Fermi liquid. Starting from the bottom of the Fermi liquid, two electrons with opposite spin occupy subsequent energy levels. In normal metals the depth of the liquid is equal to the Fermi level $e_F \approx$ O(1 eV), much larger than the thermal excitation energy $k_B T$. As a consequence, the average entropy per electron, $\bar{s}_e$, is very small and only a limited amount of electrons at the surface of the Fermi liquid is able to change kinetic states and contribute to transport. If an electron is added to such a system, only energy levels near e_F will be available and there will be a negligible change in the total entropy. As a consequence, $\mu_e \cong e_F$ is a good, first order approximation for metal electrons.

While the small polaron (Langmuir) approximation is valid for many dense membrane transition-metal oxide systems, mobile electrons in cobaltates can be described as a Fermi liquid correlated electron system in the oxygen 2p band. This system is the result of substitution, in the ideal $LaCoO_3$ perovskite structure, of divalent ions as Sr^{2+} for La^{3+}, in combination with thermal removal of oxygen at a buffered μ_{O_2}. In the resulting $La_{1-\chi}Sr_\chi CoO_{3-\delta}$ composition, the average occupation, $\bar{\theta}_{e,2p}$, of (kinetic) states in the oxygen 2p band is $(5-\chi)/(6-2\delta)$. Since the depth of the Fermi liquid increases with $\bar{\theta}_{e,2p}$, the $\mu_e \cong e_F$ of that system will also increase with $\bar{\theta}_{e,2p}$. The detailed dependence will involve the correlation between $\bar{\theta}_{e,2p}$ and the position of energy levels of the electron state. Very little progress has been made to date in usable quantitative predictions for this relation. In [27] it is shown how such information can be obtained experimentally from $\delta - \mu_{O_2}$ equilibrium data.

The assumption of mobile electrons in $La_{1-\chi}Sr_\chi CoO_{3-\delta}$ being present in kinetic states at the surface of a Fermi liquid, implies that their wave functions have long wave lengths. This is consistent with the assumption that oxygen vacancies in $La_{1-\chi}Sr_\chi CoO_{3-\delta}$ will have little effect on the thermodynamics and mobility of electrons in the oxygen 2p band.

3.3.7. Gas-solid equilibria

Expressions for gas-solid equilibria are obtained starting with:

$$\mu_{l,g} = \mu_{l,m} \tag{27}$$

For a species, *l*, that is identifiable in the gas phase. Gas-solid equilibria are particularly useful to calculate membrane feed- and permeate-side *c*'s in equilibrium with the feed- and permeate gas phase. Surface transfer limitations in thin membranes may result in deviations from (27).

3.3.8. Dense membranes

Introduction of O_2 or H_2 in the dense membrane material, does not result in a simple intercalation of the molecule but, instead, in creation or annihilization of "defect species" as shown for the incorporation of O_2 into $Fe_2O_{3-\delta}$ in (13). An equilibrium relation between p_{O_2}, δ and T is obtained by:

- Using the *p*-version of (24) for $\mu_{O_{2,g}}$.
- Obtaining Fe'_{Fe} from charge neutrality, assuming normal valences for all ions.
- Substituting in $\mu_{O_{2,g}}$ for O_2 and half-potentials for Kröger-Vink species (or complete potentials for conjugated pairs) in (13):

$$4\mu_{Fe'_{Fe}} + 2\mu_{V_O^{\cdot\cdot}} + \mu_{O_{2,g}} \rightleftarrows 4\mu_{Fe_{Fe}} + 2\mu_{O_O} \tag{28}$$

Rearrangement leads to the familiar:

$$K_{Ox} = \frac{\theta^4_{Fe_{Fe}}\theta^2_{O_O}}{\theta^4_{Fe'_{Fe}}\theta^2_{V_O^{\cdot\cdot}}p_{O_2}} = \frac{(2-2\delta)^4(3-\delta)^2}{(2\delta)^4(\delta)^2 p_{O_2}} = \exp\left(-\frac{\Delta\mu^0_{Ox}}{k_B T}\right) \tag{29}$$

In which $\Delta\mu^0_{Ox} = 4\mu^0_{Fe_{Fe}} + 2\mu^0_{O_O} - 4\mu^0_{Fe'_{Fe}} - 2\mu^0_{V_O^{\cdot\cdot}} - \mu^0_{O_2}$. Further breaking down of the right-hand μ's into h-Ts^0 leads to highly similar expressions for Δh_{Ox} and Δs^0_{Ox}. Since both are weakly T-dependent it makes sense to write:

$$K_{Ox} = K^0_{Ox}\exp\left(-\frac{\Delta h_{Ox}}{k_B T}\right) \quad \text{with}$$

$$K^0_{Ox} = \exp\left(\frac{\Delta s^0_{Ox}}{k_B}\right) \tag{30}$$

This shows that temperature dependence of K_{Ox} will largely be of the Arrhenius-type. In [31] it is shown that while $\Delta h_{Ox} =$ O(100 kJ/mole) all other, T-dependencies, when applied as a correction to Δh_{Ox} are O(10 kJ/mole).

The terms, containing δ in (29), are scaled as concentrations of species in the average $Fe_2O_{3-\delta}$ unit. The possibility of directly writing K_{Ox} in terms of pressures and concentration is one of the major assets of the Kröger-Vink notation. For ideal gas and solution equilibria, similar expressions for K in terms of concentration and $\Delta\mu^0$ can easily be written as can be derived from (23) and (24). Such expressions are sometimes referred to as "mass-action equations" while that term should actually be reserved for gaseous species with a distribution of kinetic states. Non-standard cases should always be treated with the proper μ for species involved in a reaction.

3.3.9. Micro-porous membranes

Sorption equilibria for micro-porous membranes are easily derived from a combination of (11) and (27):

$$K_l = \frac{\theta_{l,\mathrm{m}}}{(1-\theta_{\mathrm{m}})p_l} = \exp\left(\frac{-\Delta\mu_l^0}{\mathrm{k_B}T}\right) = K_l^0 \exp\left(\frac{-\Delta h_l}{\mathrm{k_B}T}\right) \quad (31)$$

When more components participate in a "competitive Langmuir" sorption equilibrium, expressions similar to (31) can be written for each component. The competitive Langmuir sorption equilibrium is particularly useful for separations involving larger molecules with zeolite membranes. With only one component l present, (31) can be written into a more familiar expression for the single component Langmuir isotherm:

$$\theta_{l,\mathrm{m}} = \frac{K_l p_l}{1 + K_l p_l} \quad (32)$$

When $\theta_{\mathrm{m}} \to 0$ in (31), the $(1-\theta_{\mathrm{m}})$ term can be dropped and:

$$K_l = \frac{\theta_{l,\mathrm{m}}}{p_l} \quad (33)$$

The Henri sorption equilibrium (33) is useful to obtain very simple transport equations in many membrane processes with $\theta_{\mathrm{m}} \to 0$. An example is light molecule separation with amorphous silica membranes. However, the validity of (33) should always be verified up front.

3.3.10. Ion-solid interface equilibria in solutions

Equilibria between dissolved species and solid surfaces are important for:

- The understanding of colloid stability, in turn, relevant for synthesis of membrane and support layers by colloidal processing [2].
- Transport of solutions through meso- and macroporous structure.

There is an overwhelming amount of literature about this subject in physical chemistry. We will restrict to a very brief discussion of ions dissolved in polar liquids, ℓ, primarily water in equilibrium with insoluble inorganic solids. The solid/liquid interface, sℓ, often shows preferential adsorption of specific ions. A common example is preferential adsorption of protons. This leads to an excess positive surface charge and surface potential with respect to the bulk solution. The excess surface charge is compensated by a "diffuse cloud" near the surface of excess negative charge in the solution. This excess charge, $\sum z_l c_l$, is the result of $\sum z_{l^-} c_{l^-}$ being slightly larger than $\sum z_{l^+} c_{l^+}$ for mobile ions near the surface, without significantly affecting c. The excess is evened out by thermal equilibration over a characteristic "Debye length", which for a flat surface equals:

$$\frac{1}{\kappa} = \sqrt{\frac{2\mathrm{F}^2 I^{\mathrm{c}}}{\varepsilon_0 \varepsilon_{\mathrm{r}} \mathrm{R}T}} \quad (34)$$

The Debye length is O(10 nm) in dilute aqueous solutions. The DLVO theory is commonly used to explain the stability of charged colloids as a function of surface potential, I^{c} and T. It also provides the insight, demonstrated in Fig. 4, that ionic aqueous solutions in meso-pores with $r_{\mathrm{p}} < 1/\kappa$ have an excess charge, present over the entire pore volume.

More quantitative predictions of colloidal stability and excess charge in membrane pores can be done with the "charge regulation" treatment [32]. This treatment considers selective adsorption of ions with an ideal Langmuir lattice μ as in (11), in combination with a μ as in (23) for mobile ions near the interface. In both cases a non-trivial electric potential energy needs to be included:

$$\mu_{l,\mathrm{s}\ell} = \mu_{l,\mathrm{s}\ell}^0 + \mathrm{k_B}T \ln\left(\frac{\theta_{l,\mathrm{s}\ell}}{1-\theta_{\mathrm{s}\ell}}\right) + z_l \mathrm{q_{el}} \Phi(0) \quad (35)$$

$$\mu_{l,\ell} = \mu_{l,\ell}^0 + RT \ln\left(\frac{\gamma_{l,\ell} c_{l,\ell}}{c^0}\right) + z_l \mathrm{q_{el}} \Phi(y) \quad (36)$$

Solutions for c and Φ(y) are obtained for specific geometries by setting (35) and (36) equal for each charged species at all locations, charge balance and Poisson's relation:

$$\Delta\Phi = -\frac{\mathrm{F}}{\varepsilon_0 \varepsilon_{\mathrm{r}}} \sum_{l=1}^{l=l^{\max}} z_l c_l \quad (37)$$

More detailed treatments consider multilayer sorption, for instance by specific ions on the first lattice, created by selective proton sorption. Single- and dual layer descriptions involving protons are known as the 1-p_{K} and 2-p_{K} models [33].

3.3.11. Buffering of gas phase and ion equilibria

The $p_{\mathrm{O_2}}$ in equations like (29) should primarily be read as a mathematical representation of $\mu_{\mathrm{O_{2,g}}}$. This "effective $p_{\mathrm{O_2}}^{\mathrm{eff}}$" may have a wide range of values between 10^{-40} and 5×10^7 Pa. The lower pressures in this range cannot be realized with real O_2 molecules. However, pressures >10 Pa can be realized with O_2 molecules, possibly in mixtures with inert N_2.[10] Pure gases, l, possibly mixed with inert are further indicated as l/inert. Lower values for $p_{\mathrm{O_2}}^{\mathrm{eff}}$ can be realized at high T with CO/CO_2/inert and even lower in H_2/H_2O/inert and with CO/inert in the presence of solid carbon. In

[10] Pure O_2 at pressures $>10^5$ Pa provide a serious safety risk and the highest pressures are seldom found in a laboratory environment.

these mixtures, $\mu_{O_{2,g}}$ is established in:

$$2CO\,(g) + O_2 \rightleftarrows 2CO_2\,(g)$$
$$\rightarrow \mu_{O_2} = 2\mu_{CO_{2,g}} - 2\mu_{CO,g} \quad (38)$$
$$2H_2\,(g) + O_2 \rightleftarrows 2H_2O\,(g)$$
$$\rightarrow \mu_{O_2} = 2\mu_{H_2O,g} - 2\mu_{H_{2,g}} \quad (39)$$
$$2C\,(s) + O_2 \rightleftarrows 2CO\,(g)$$
$$\rightarrow \mu_{O_2} = 2\mu_{CO,g} - 2\mu_{C,s} \quad (40)$$

When the pressures of the gases in (38)–(40) are kept constant, a T-dependent $p^{\text{eff}}_{O_2}$ results. In addition, the reactivity of the components of the gas mixture should be considered:

- CO_2 is known to form very stable $BaCO_3$ with Ba-compounds.
- H_2O may react with La-compounds at low T to form La-oxyhydroxides.

It is experimentally very difficult to apply (38)–(40) all in one single process and, even if that would be possible fit would be unable to cover the complete lower $p^{\text{eff}}_{O_2}$ range. In any case the use of $p^{\text{eff}}_{O_2}$ in reaction equilibria is only meaningful when sufficient amounts of reactive species are present in the gas phase to deal with small intra- and extra-mural gas leaks and to accommodate sufficient gas-solid exchange of species to maintain the equilibrium. Drawing a parallel, in aqueous chemistry this is known as "p_H buffering" with the p_H being just a mathematical transformation of $\mu_{H^+,aq}$. Similar to p_H buffering we define a buffer-capacity for gaseous species l:

$$\beta_l = RT\frac{dc^t_l}{d\mu_l} \quad (41)$$

In which dc^t_l refers to an infinitesimal amount of added species l, expressed as a concentration. One can add, for instance, a small amount of O_2 to a buffered CO/CO_2 mixture; the real c_{O_2} before and after the addition will be very small and hardly change. Justifying the need of adding another superscript, $dc^t_{O_2}$ is just that small amount of real O_2 added, divided by the volume of CO/CO_2 mixture. β_j has the dimension of c.

For l/inert:

$$\beta_l = c_l \quad (42)$$

For l_1/l_2/inert with $l_1 = CO|H_2$ and $l_2 = CO_2|H_2O$ a combination of (24), (38), (39) and (41) leads to:

$$\beta_{O_2} = \frac{c_{l_1}c_{l_2}}{4\left(c_{l_1} + c_{l_2}\right)} \quad (43)$$

Which has a maximum at $\beta^{\max}_{O_2} = c_l/8$ when $c_{l_1} = c_{l_2}$. From experimental observations, gases well buffered for l have:

$$\beta_l \gg 10^{-3}\ \text{mole/m}^3 \quad (44)$$

Which for l/inert corresponds to $p_l \gg 0.01T$ Pa and for equimolar l_1/l_2/inert mixtures, discussed before, to $p_l \gg 0.1T$ Pa.

In membrane transport measurements, buffering may become an issue, in particular at the feed side where lower p_l's are maintained. In dense membrane measurements, O_2 buffering is a major concern for both the feed and the permeate side. In that case $\beta_l < 10^{-3}$ mole/m^3 definitely leads to meaningless results. Microporous membrane measurements may allow for an unbuffered permeate atmosphere (inert sweep or vacuum) if $c^p_{l,m} = 0$ can be maintained unambiguously at that level.

For ions in solution (41) provides a good definition too, and the same practical limits for a well-buffered system. However, the accepted definition for p_H is $\log_{10}$ based and differs by a factor of ln 10.

3.4. Diffusion permeation

Knowledge of detailed expressions for the μ of mobile species is a first important step in irreversible thermodynamic treatments of mass transport by using Onsager (or Maxwell-Stefan) equations. In addition, thermodynamic treatments can be confronted with fully microscopic treatments for verification and connection of phenomenological parameters with microscopic parameters.

In this section we will restrict to diagonal Onsager treatments. Cases such as multi-component transport of ionic solutions and gas mixtures through meso- and macro-pores, for which this approximation cannot be made, are better treated with the Maxwell-Stefan formalism [26, 33]. In the next sections, various manifestations of single-species diffusion will be used to create a set of internally consistent and unambiguous definitions for the three major classes of diffusion coefficients: the chemical $\tilde{D}$, the component D and the self D^s.

3.4.1. Single species chemical diffusion on an ideal Langmuir lattice

Solution of diagonal Onsager equations for species l requires knowledge of μ_l and b_l. One of the more illustrative examples is the case of stationary single species chemical diffusion on an ideal Langmuir lattice. This quasi-binary system is relevant for single component and low-c multi-component permeation through microporous materials *and* part of the story in mixed conduction. We will cast our result in the form of Fick's first law:[11]

$$j_l = -\tilde{D}_l\nabla c_l \quad (45)$$

Combination of (9), (10), molar form of (11), and $c_j = \theta_j c^{\text{tot}}$ leads to:

$$j_l = -\tilde{f}_L b^0_l(1-\theta_l)\theta_l c^{\text{tot}}\nabla\left[RT\ln\left(\frac{\theta_l}{1-\theta_l}\right)\right]$$
$$= -\tilde{f}_L b^0_l RT\nabla c_l \quad (46)$$

[11] From which all diffusion coefficients are eventually derived.

In (46), the $(1-\theta_l)$ term in b_l just cancels out against the Darken thermodynamic factor:

$$\Gamma_l = \frac{c_l}{\mathrm{R}T}\frac{d\mu_l}{dc_l} = \frac{1}{1-\theta_l} \tag{47}$$

Combination of (45) and (46) leads to an easy identification of:

$$\tilde{D}_l = \tilde{f}_L b_l^0 \mathrm{R}T \tag{48}$$

This result could also have been obtained in an ideal diluted system with $\tilde{f}_L \to 1$, $\theta \to 0$ and hence (18), and (10) $\to b_l = b_l^0$. However, (46) is more general and covers both the ideal diluted solution and Langmuir systems. And, because many systems can be described as a Langmuir system, it explains why $\tilde{D}$ is often really a constant.

Simulations show that $\tilde{f}_L \to 1$ at significant $\nabla\theta_l$ [24] with the expectation that $\tilde{f}_L \to f_L^{\mathrm{s}}$ for $\nabla\theta_l \to 0$. If that is the case indeed there is no real concern with $\tilde{f}_L$ providing a small correction for the not very relevant $\nabla\theta_l \to 0$ case *and* taking into account the limited accuracy at which $\tilde{D}$ is generally obtained. However, $\tilde{f}_{l,L}$ may reduce b_l very significantly in chemical multi-component diffusion as explained in Section 3.4.3.

3.4.2. Single species field-driven diffusion in an ideal Langmuir lattice

The next case is that of a single species field-driven conductive diffusion in an ideal Langmuir lattice. This case is relevant for conduction in solid electrolyte membranes and, again, part of the story in mixed conduction.

In electrolytes, θ_l is independent of x. Ignoring electrode effects and build-up of space-charge at interfaces we may assume the electrolyte to behave like a normal dielectric and a voltage difference $\Delta\Phi_{\mathrm{fp}}$, applied to both sides of the membrane will result in a constant $\nabla\Phi = \Delta\Phi_{\mathrm{fp}}/X$ inside the membrane. The chemical potential for the mobile species can be obtained by including the electrical potential in the molar form of (11):

$$\mu_l = \mu_l^0 + \mathrm{R}T\ln\left(\frac{\theta_l}{1-\theta_l}\right) + z_l\mathrm{F}\Phi \tag{49}$$

Application of (9) and θ_j independent of x then leads to the thermodynamic version of Ohm's law:

$$j_l = b_l c_l \nabla z_l \mathrm{F}\Phi \tag{50}$$

Since $\nabla z_l \mathrm{F}\Phi$ is constant we can create a new, component diffusion coefficient, D_l, by drawing the analogy with (48):

$$D_l = b_l \mathrm{R}T \quad \left(\text{note } b_l,\ \text{not } b_l^0\right) \tag{51}$$

Equation 51 is known as the Nernst-Einstein relation and we actually use it here as a defining relation for D. The rationale can be found in ideal systems where the difference between b_l and b_l^0 disappears and eventually $D = \tilde{D}$. Considerations involving the l, V jump balance suggests that $f_L = 1$ in any case for single species field-driven diffusion but the author is not aware of a formal proof of that statement. However, $f_{l,L}$ may reduce b_l very significantly in field-driven multi-component diffusion as is explained for chemical multi-component diffusion in the next section.

3.4.3. 2-Component chemical diffusion on an ideal Langmuir lattice

In each of the previous cases we included a defining equation for one of the major classes of diffusion coefficients. The case of 2-component chemical diffusion in an ideal Langmuir lattice will lead to the third: the self-diffusion coefficient D^{s} as discussed in the next section in quite an unusual way. This quasi-ternary system is relevant for separation of components from a mixture by permeation through micro-porous materials *and* in which more than one mobile component is present in the membrane.

Combination of (9), (10), molar form of (11), and $c_j = \theta_j c^{\mathrm{tot}}$ leads to:

$$j_{l_1} = -\tilde{f}_{l_1,L} b_{l_1}^0 (1-\theta)\theta_{l_1} c^{\mathrm{tot}} \nabla\left[\mathrm{R}T\ln\left(\frac{\theta_{l_1}}{1-\theta}\right)\right] \tag{52}$$

With $\theta = \theta_{l_1} + \theta_{l_2}$, this can be worked out as:

$$j_{l_1} = -\tilde{f}_{l_1,L} b_{l_1}^0 \mathrm{R}T\left[\left(1-\theta_{l_2}\right)\nabla c_{l_1} + \theta_{l_1}\nabla c_{l_2}\right] \tag{53}$$

And using symmetric exchange of 1 and 2:

$$j_{l_2} = -\tilde{f}_{l_2,L} b_{l_2}^0 \mathrm{R}T\left[\theta_{l_2}\nabla c_{l_1} + \left(1-\theta_{l_1}\right)\nabla c_{l_2}\right] \tag{54}$$

In this case we kept the non-equilibrium correlation coefficients, $\tilde{f}_{l,L}$, because, as is shown in [24] for mixtures of fast l_1 and slow l_2, $\tilde{f}_{l_1,L} \to 0$. This is explained by the observation that all fast l_1 in a gradient will eventually meet a slow l_2, not making way. The limiting case of $b_{l_2}^0 = 0$ can be used as a model for single gas permeation through amorphous silica membranes. In that case, small immobile silica units, l_2 (corner-sharing SiO_4 tetrahedra) are distributed at random over an imaginary Langmuir lattice with $\theta_{l_2} = \mathrm{O}(0.5)$. An uncorrelated (53) would for that case predict a significant permeation with θ_{l_2} above the site percolation limit of 0.67. A detailed simulation revealed the correct percolation behavior for l_1 as can be incorporated in (53) with the proper values for $\tilde{f}_{l_1,L}$. [24]

Equations 53 and 54 can be combined in a "multi-component diffusion matrix" notation as follows:

$$\mathbf{j}_l = \tilde{\mathbf{D}}_l \nabla \mathbf{c}_l \quad \text{or} \quad \begin{pmatrix} j_{l_1} \\ j_{l_2} \end{pmatrix} = \begin{pmatrix} \tilde{D}_{l_1 l_1} & \tilde{D}_{l_1 l_2} \\ \tilde{D}_{l_2 l_1} & \tilde{D}_{l_2 l_2} \end{pmatrix} \begin{pmatrix} \nabla c_{l_1} \\ \nabla c_{l_2} \end{pmatrix} \tag{55}$$

In which $\tilde{D}_{l_1 l_1} = \tilde{f}_{l_1,L} b_{l_1}^0 \mathrm{R}T(1-\theta_{l_2})$, $\tilde{D}_{l_1 l_2} = \tilde{f}_{l_1,L} b_{l_1}^0 \mathrm{R}T\theta_{l_1}$, $\tilde{D}_{l_2 l_1} = \tilde{f}_{l_2,L} b_{l_2}^0 \mathrm{R}T\theta_{l_2}$, and $\tilde{D}_{l_2 l_2} = \tilde{f}_{l_2,L} b_{l_2}^0 \mathrm{R}T(1-\theta_{l_1})$, demonstrating that, contrary to the

Onsager transport coefficient matrix, $\mathbf{L}_l$, such a "multi-component diffusion matrix" is not symmetric. The "multi-component diffusion matrix" of (55) should not be confused with the symmetric "single component directional diffusion matrix," $\mathbf{j}_x = \tilde{\mathbf{D}}_x \nabla \mathbf{c}_x$, used to calculate fluxes for various directions in an anisotropic structure. $\tilde{\mathbf{D}}_x$ is isotropic for cubic and amorphous structures, in which the $\tilde{\mathbf{D}}_l$ of (55) can be used for all directions. $\tilde{\mathbf{D}}_x$ is not isotropic for the lower-than-cubic symmetries as often occur in zeolites. Combining $\tilde{\mathbf{D}}_l$ and $\tilde{\mathbf{D}}_x$ for those symmetries will be an interesting mathematical exercise that may have some relevance in simplifying the very complicated problem of multi-component diffusion in normal polycrystalline, lower symmetry zeolite membranes.

3.4.4. Self-diffusion in an ideal Langmuir lattice

The idea behind self-diffusion is to express mobility of species in terms of a self-diffusion coefficient, D^{s}. The relevance for membranes is:

- To make the diffusion coefficient picture complete.
- To offer tools to translate D^{s} from experiments or computer simulations into $\tilde{D}$ or D.

It is a priori impossible to connect D^{s} directly with b since that quantity was invented to connect non-equilibrium driving forces with fluxes. The normal approach to obtain D^{s} is to follow the time-averaged correlated random walk of tracer species, initially present on a plane on or inside a piece of matter. The tracers can be real or simply labeled and tracked in an imaginary registry. The physical labeling creates a true non-equilibrium system that bears great similarity to the artificial non-equilibrium system with logical tracers. The time-dependent Gaussian diffusion profile that results from the random walk is compared with the well known Gaussian chemical diffusion profile of the tracer, resulting in:

$$D^{\mathrm{s}} = f_L^{\mathrm{s}} b_0 (1-\theta) RT \tag{56}$$

This result can also be obtained in an imaginary experiment of stationary logical tracer diffusion of l^* through a membrane in which $\theta_{l^*}^{\mathrm{f}}$ and $\theta_{l^*}^{\mathrm{p}}$ are kept at different but constant values by renaming normal species into tracers and vice versa. (53) becomes:

$$j_{l^*} = -\tilde{f}_{l^*,L} b_{l^*}^0 \mathrm{R}T\left[(1-\theta_l)\nabla c_{l^*} + \theta_{l^*}\nabla c_l\right] \tag{57}$$

The fact that l and l^* have identical properties leads to: $\nabla c_{l^*} = -\nabla c_l$, $\tilde{f}_{l^*,L} = \tilde{f}_L$ and (57) rearranged into:

$$j_{l^*} = -\tilde{f}_L b_{l^*}^0 (1-\theta)\,\mathrm{R}T\nabla c_{l^*} \tag{58}$$

Comparison of this result with Fick's law (45), followed by $D^{\mathrm{s}} = \tilde{D}_{l^*}$ and $\tilde{f}_L = f_L^{\mathrm{s}}$ results in (56).

Self-diffusion coefficients, obtained with physical isotope tracers require a small mass correction, for the simplest case:

$$D^{\mathrm{s}} = \sqrt{\frac{m_l}{m_{l^*}}}\tilde{D}_{l^*} \tag{59}$$

3.4.5. Two-component mixed conduction on interpenetrating Langmuir lattices

The case of two-component mixed conduction on interpenetrating Langmuir lattices focuses on the mixture of chemical and internal field-driven diffusion as occurs in O_2 permeation through dense perovskite membranes. In that case:

- O^{2-} transport takes place by substitutional vacancy diffusion on the O_O sub-lattice.
- Compensating electronic conduction takes place on either the O_O sub-lattice or a multivalent cation sub-lattice.

The presence of both an internal diffusion field and a ∇c_V makes this case more complicated than the previous ones. Both conductors on the same sub-lattice would result in significant cross-coefficients and, to date, little progress has been made to address this in a systematic way. One of the most complete analyses is found in [34] for $La_{0.8}Sr_{0.2}CoO_{3-\delta}$ in which an overall transport equation is presented as:

$$J_{\mathrm{O}_2} = -L_{\mathrm{O}_2}\nabla\mu_{\mathrm{O}_2} \tag{60}$$

$$L_{\mathrm{O}_2} = \left(\frac{4}{c_{\mathrm{O}^{2-}} b_{\mathrm{O}^{2-}}} + \frac{16}{c_e b_{\mathrm{e}}}\right)^{-1} \tag{61}$$

$$\mu_{\mathrm{O}_2} = e_{\mathrm{O}_2} - T s_{\mathrm{O}_2} \tag{62}$$

The term e_{O_2} shows a dependence on $\theta_{\mathrm{O_O}}$ that is attributed to change in e_{F} of the Fermi liquid correlated electron system in the oxygen 2p band. Changes in s_{O_2} with $\theta_{\mathrm{O_O}}$ can be attributed to the configurational entropy of $V_{\mathrm{O}}^{\cdot\cdot}$. (61) is obtained with an ambipolar diffusion treatment. The common assumption that $b_e \gg b_{\mathrm{O}^{2-}}$ leads to the simpler result:

$$L_{\mathrm{O}_2} = \frac{c_{\mathrm{O}^{2-}} b_{\mathrm{O}^{2-}}}{4} \tag{63}$$

This quantity is a function of $\theta_{\mathrm{O_O}}$ and hence of x. Detailed treatments in which this effect is taken into account have not been reported in literature. Diffusion correlation effects are likely to be complicated, but unimportant.

4. Concluding remarks

In real-life applications in separation or reactor modules, the membranes and their (support) morphology along with their bc values are only (an important) part of the story. The overall transport of the species considered will also depend on external mass transfer limitations (in boundary layers), details of transport mechanisms in porous supports whenever present, surface

transfer kinetics and macroscopic changes of temperature and concentrations with time and location in the reactor design. Target applications will provide additional boundary conditions for the entire membrane module such as thermo-chemical stability, mechanical properties such as the ability to withstand large pressure differences and compatibility with other parts. The latter includes dimensional tolerances, surface roughness and the possibility of sealing. Cost-competitive inorganic membrane system designs will finally be the result of a complete optimization involving all aspects mentioned [35]. So in future programs membrane (module) synthesis (manufacturing) will be considered more and more with target applications and all boundary conditions in mind. This means that we will face the following challenges:

- Exploration of advanced synthesis options for membrane and support modules.
- Determination of consistent, accurate intrinsic membrane transport parameters.
- Developing more integrated transport modeling tools for experimental and application-oriented membrane systems using modern computational methods considering all relevant lengths scales (multi-scale modeling).

Acknowledgements

The author is indebted MS and PhD students and coworkers at the University of Twente and The Ohio State University, who have contributed to the results summarized in this paper. Among these, I like to mention in particular N.E. Benes, P.M. Biesheuvel, A.J. Burggraaf, J.E. ten Elshof, L.M. van der Haar, H. Kruidhof, M.H.R. Lankhorst, W.B.S. de Lint, A. Nijmeijer, G.T. Quickel, R.M. de Vos, D. Yu, V.W. Verweij for Fig. 8 and X. Cao for Fig. 10.

List of Symbols

In a recent discussion I had with a prominent member of the membrane community he described the developing collection of symbols used in the membrane field as "alphabet soup". Notations for different types of diffusion coefficients form a class of their own. Below I present the ingredients of my soup. In defining symbols I use the following rules:

- Roman and lower case Greek variables are set in *italic* and vector quantities in **bold**. All others, constants, functions, chemical symbols and texts are set in regular.
- The notation for a quantitative variable, S, is $S^{\text{specific state,reference frame}}_{\text{species, location}}$.
  - Whenever appropriate, the main symbol will be in upper case (S) if it describes numbers of atomic/molecular species *and* in lower case (s) if it describes numbers of moles; a particle flux will be J and a molar flux will be j. Many intensive/extensive parameters will be in lower case/upper case and thermodynamic properties of atomic species (e, h, s) in lower case.
  - The *species* subscript is self-explanatory, it may refer to the species in a chemical potential or mobile entities in transport.
  - The *location* subscript can be a phase such as gas (g), liquid (ℓ), pore (p) or solid (s) or specify part of a supported membrane structure such as the actual membrane (m), the support top layer (u_1), etc.
  - The *specific state* superscript can refer to the variable at certain conditions. This is often the variable at a certain standard or initial state. Examples are the chemical potential at standard conditions, μ^0, or the (unconditional) mobility, b^0.
  - The *reference frame* superscript is typical for transport coefficients that can be defined with respect to different reference frames such as the lattice (L) or the molar average (M).
  - Specific sub- or superscripts are left out if they are not applicable or the main variable covers a full range of sub- or superscript values. Leading comma's are discarded.
  - Multiple sub- or superscripts may be separated by comma's.
  - One example of a parameter for which all sub- and superscripts apply is $b^{0,\mathrm{L}}_{\mathrm{O^{2-}},\mathrm{m}}$, the unconditional mobility with respect to the lattice reference frame for O^{2-} in a membrane. In this paper we consider exclusively the lattice frame and hence leave it out.
- Alphabets with only 24 Greek and 26 Roman letters make collisions unavoidable. Local variables are sometimes used, like in computer programming, only defined in one line or section where they are used.

Global symbols and abbreviations used in this paper

Greek

β	Buffer capacity.
χ	Cation substitutional composition parameter.
Δ	Difference.
δ	Deviation from the ideal stoichiometry in a compound.
ε_0	Dielectric constant of vacuum.
ε_r	Relative dielectric constant.
Φ	Electrical potential.
ϕ	Volume fraction.
Γ	Darken thermodynamic factor.
γ	Activity coefficient to be used as correction to the concentration term in common expressions for μ (not recommended).
ι	Exponent of r_p, in expressions for transport resistance in meso- and macro-porous structures. $\iota = 1$ for pure Knudsen flow (of gases) and $\iota = 2$ for viscous flow (of gases and mixtures). In qualitative considerations $1 \leq \iota \leq 2$ may be used to indicate gas flow in structures with defects *and* for the regime of transition between Knudsen and viscous flow.
κ	Inverse Debye length.

θ Time-averaged occupation of a site in a dense structure that is available to accommodate one mobile species. Also used for occupation of kinetic states in an electronic band of finite width.
σ Stress in solid.
τ Tortuosity, defined as the ratio of average transport length and projected parallel length in a certain direction.
μ Molar or particle chemical potential, *exclusive* of any $q\Phi$ term. The type should be clear from the context.
μ^0 Part of μ, exclusive of partial entropy due to distribution over locations or kinetic states.
$\tilde{\mu}$ Chemical potential, *inclusive* of any $q\Phi$ term.

Abbreviations, chemical symbols, constants, functions, and operators

0 When used as a superscript, refers to a standard state of the variable.
d Differential d.
DLVO Derjaguin-Landau-Verweij-Overbeek (well-known acronym for classical theory for colloid stability; V and O were both Dutch, but V is no immediate relative of the author).
def Defect.
disp State for particles, dispersed in a liquid or solid or present in a "green" compact. The latter is achieved by cold, non-reactive consolidation of particles. It is generally assumed that the transition from a precursor composition to a final composition does not lead to significant dimensional effects or that it is corrected for.
e Normal metal mobile electron.
eff Effective (used when a quantity represents a mathematical transformation with similar properties).
ext External (source in a solid state chemical reaction equation).
FIB Focused Ion Beam.
F Faraday's constant.
f Feed-side superscript constant.
grain Grain in a poly-crystalline structure.
h Planck's constant.
k_B Boltzmann constant.
ℓ Liquid phase.
m Membrane ($m = u_0$).
max Maximum.
min Minimum.
MS Maxwell-Stefan description for transport processes.
N_{Av} Avogadro's number.
$O(x)$ Returns the order of magnitude of local variable x.
opt Optimized.
f Permeate-side superscript constant.
p Pore subscript constant.
q_{el} Elementary charge.
qh Quasi-homogeneous, used for defect-free porous structures that appear homogeneous over $5r_s^{disp}$.
R Gas constant.
s Dense crystalline, amorphous or quasi-homogeneous solid.
TEM Transmission Electron Microscopy.
t Superscript variable, indicating the total amount of added species.
u Support layer.
$\hat{V}$ Notation for vacancies to which a model-based complete chemical potential can be assigned. A site subscript may be added as in the Kröger-Vink notation but the ^ sign is added to distinguish from the normal Kröger-Vink vacancy.

Roman variables

A Exposed membrane surface.
b Mechanical mobility.
b^0 Unconditional b (All neighboring sites are available for diffusion hopping transport).
$C|c$ Particle|molar concentration.
c^0 Standard c, for instance 1 mole/m^3.
$\tilde{D}$ Chemical diffusion coefficient.
D Component diffusion coefficient.
D^s Self-diffusion coefficient.
e Partial particle energy.
e_F Fermi energy.
$\bar{F}$ Thermodynamic driving force.
f_L^s Bardeen-Herring quasi-equilibrium diffusion correlation coefficient for a lattice L. $0.5 < f^s < 1$ for $\theta \to 1$ in any lattice type; f^s tends towards unity at decreasing θ.
$\tilde{f}_L$ Non-equilibrium correlation coefficient for chemical diffusion on a lattice L. In single-component mixtures $0.5 < \tilde{f}_L < 1$ for $\theta \to 1$ expected. In multi-component mixtures $0 < \tilde{f}_{l,L} < 1$; $\tilde{f}_{l,L}$ tends towards unity with decreasing θ.
f_L Non-equilibrium correlation coefficient for field-driven diffusion on a lattice L. In single-component mixtures $f_L = 1$ expected. In multi-component mixtures $0 < f_{l,L} < 1$; $f_{l,L}$ tends towards unity with decreasing θ.
g Multiplicity of particles in degenerate states.
h Partial particle enthalpy.
$J|j$ Particle|molar; $J|j = N|n/A$.
K Equilibrium constant.
k Support layer index. In a multi-layer structure, k ranges from 1, for the top-layer that supports the membrane, to the total number of layers, k_{max}.
L Lattice variable.
L_l Diagonal Onsager transport coefficient for species l in systems where all cross-coefficients are 0.
L_{l_1,l_2} Onsager transport coefficient for species l_1 and l_2.
l Mobile species.
l^* Labelled l. The labeling can be done by simply registering the species in an ensemble

	(in computer simulations by naming and tracking) or by using a specific isotope of *l* (in *real* experiments).
m	Particle mass.
m^*	Effective thermal mass for free electrons and holes in normal, lightly doped semiconductors.
$N \mid n$	Particle | molar flow.
p	Gas pressure.
p^0	Standard p, for instance 1 bar or 1 Pa.
q	Electrical charge.
R	Molecular formula of the average primitive cell of a solid, representative for the chemical composition of a solid.
r	Radius.
s	Partial particle entropy.
s^0	Part of s, exclusive of contribution due to distribution over locations or kinetic states.
$\bar{v}$	Time-average velocity.
X	Membrane, support layer thickness.
x	Distance coordinate within a supported membrane structure with direction perpendicular to the membrane, origin at the membrane surface and positive within the supported structure.
y	Distance coordinate within a liquid near a solid interface with direction perpendicular to the interface, origin at the interface and positive within the support structure.
z	Charge of ionic or electronic species, expressed in units of q_{el}.

References

1. R. R. BHAVE, "Inorganic membranes, Synthesis, Characteristics and Applications" (Van Nostrand Reinhold, New York, 1991).
2. H. VERWEIJ, "Novel Synthesis of Ceramic Membranes," in Proc. 10th Int. Ceramics Congres & 3rd Forum on New Materials, Session J-4, Florence, Italy, July 14–18, 2002.
3. L. M. VAN DER HAAR, "Mixed-conducting perovskite membranes for oxygen separation—Towards the development of a supported thin film membrane," Thesis, University of Twente, Enschede, The Netherlands 2001.[12]
4. Y. S. LIN and A. J. BURGGRAAF, *J. Membrane Sci.* **79**(1) (1993) 65.
5. A. NIJMEIJER, H. KRUIDHOF, R. BREDESEN and H. VERWEIJ, *J. Amer. Ceram. Soc.* **84**(1) (2001) 136.
6. R. M. DE VOS and H. VERWEIJ, *Science* **279** (1998) 1710.
7. Y. LU, G. CAO, R. P. KALE, S. PRABAKAR, G. P. LOPEZ and C. J. BRINKER, *Chem. Mater.* **11** (1999) 1223.
8. H. VERWEIJ, G. DE WITH and D. VEENEMAN, *J. Mater. Sci.* **20**(3) (1985) 1069.
9. C. J. M. VAN RIJN, W. NIJDAM, S. KUIPER, G. J. VELDHUIS, H. A. G. M. VAN WOLFEREN and M. C. ELWENSPOEK, *J. Micromech. Microengin.* **9**(2) (1999) 170.
10. F. C. M. WOUDENBERG, W. F. C. SAGER, N. G. M. SIBELT and H. VERWEIJ, *Adv. Mater.* **13**(7) (2001) 514.
11. J. REYES-GASGA, T. KREKELS, G. VAN TENDELOO, J. VAN LANDUYT, W. H. M. BRUGGINK, H. VERWEIJ and S. AMELINCKX, *Sol. St. Comm.* **70**(4) (1989) 269.
12. C. S. CHEN, H. KRUIDHOF, H. J. M. BOUWMEESTER, H. VERWEIJ and A. J. BURGGRAAF, *Solid State Ionics* **86/88**(1) (1996) 569.
13. For IZA zeolite structure acronyms see: http://www.iza-structure.org/databases/.
14. Z. P. LAI, G. BONILLA, I. DIAZ, J. G. NERY, K. SUJAOTI, A. M. AMAT, E. KOKKOLI, O. TERASAKI, R. W. THOMPSON, M. TSAPATSIS and D. G. VLACHOS, *Science* **300**(5618) (2003) 456.
15. Y. F. LU, R. GANGULI, C. A. DREWIEN, M. T. ANDERSON, C. J. BRINKER, W. L. GONG, Y. X. GUO, H. SOYEZ, B. DUNN, M. H. HUANG and J. I. ZINK, *Nature* **389**(6649) (1997) 364.
16. D. ZHAO, P. YANG, N. MELOSH, J. FENG, B. F. CHMELKA and G. D. STUCKY, *Adv. Mater.* **10**(16) (1998) 1380.
17. C. Y. TSAI, S. Y. TAM, Y. F. LU and C. J. BRINKER, *J. Membrane Sci.* **169**(2) (2000) 255.
18. H. XU and W. A. GOEDEL, *Langmuir* **18**(6) (2002) 2363.
19. P. M. BIESHEUVEL, V. BREEDVELD, A. P. HIGLER and H. VERWEIJ, *Chem. Eng. Sci.* **56**(11) (2001) 3517.
20. J. E. SMAY, J. CESARANO and J. A. LEWIS, *Langmuir* **18**(14) (2002) 5429.
21. X. HAN, K. W. KOELLING, D. L. TOMASKO and L. J. LEE, *Polym. Eng. Sci.* **42**(11) (2002) 2094.
22. M. H. R. LANKHORST, H. J. M. BOUWMEESTER and H. VERWEIJ, *J. Amer. Ceram. Soc.* **80**(9) (1997) 2175.
23. N. BENES and H. VERWEIJ, *Langmuir* **15**(23) (1999) 8292.
24. N. E. BENES, H. J. M. BOUWMEESTER and H. VERWEIJ, *Chem. Eng. Sci.* **57**(14) (2002) 2673.
25. N. E. BENES, G. SPIJKSMA, H. VERWEIJ, H. WORMEESTER and B. POELSEMA, *AIChE J.* **47**(5) (2001) 1212.
26. N. E. BENES, Mass Transport in Thin Supported Silica Membranes, Thesis, University of Twente, Enschede, The Netherlands, 2001.
27. M. H. R. LANKHORST, H. J. M. BOUWMEESTER and H. VERWEIJ, *Phys. Rev. Lett.* **77**(14) (1996) 2989.
28. W. SCHOTTKY, "Halbleiterprobleme," Vol. IV, 235 (1958).
29. C. W. DAVIES, "Ion Association" (Butterworths, London, 1962) p. 41.
30. R. M. DE VOS and H. VERWEIJ, *J. Membrane Sci.* **143**(1) (1998) 37.
31. H. VERWEIJ, W. H. M. BRUGGINK, R. A. STEEMAN, E. FRIKKEE and R. B. HELMHOLDT, *Physica C* **166**(4) (1990) 372.
32. P. M. BIESHEUVEL, *Langmuir* **17**(12) (2001) 3553.
33. W. B. S. DE LINT, Transport of Electrolytes through Ceramic Nanofiltration Membranes, Thesis, University of Twente, Enschede, The Netherlands, 1997.
34. M. H. R. LANKHORST, Thermodynamic and transport properties of mixed ionic-electronic conducting perovskite oxides, Thesis, University of Twente, Enschede, The Netherlands, 1997.
35. P. M. BIESHEUVEL and H. VERWEIJ, *J. Membrane Sci.* **156** (1999) 141.

[12] Most of the University of Twente theses are currently available as pdf downloads on http://www.ub.utwente.nl/webdoc/docs/ct.shtml.